nature portfolio

Peer Review File

Tetravalent organic cation-enabled dual interfacial regulation for durable aqueous zinc–iodine batteries

Corresponding Author: Professor Jijian Xu

This file contains all reviewer reports in order by version, followed by all author rebuttals in order by version.

Version 0:

Reviewer comments:

Reviewer #1

(Remarks to the Author)
This work proposes the use of a high-valent organic cation (HVOC) to construct dual interfaces for improving the stability of Zn–I2 batteries, and the results demonstrate promising performance. However, several important issues need to be clarified. The synthesis of the HVOC molecule is complicated and costly, raising doubts about its practical applicability. On the experimental side, the use of Zn(OTF)2 instead of more economical ZnSO4 lacks justification, the rationale behind the HVOC concentration under high loading iodine is not explained, and the initial capacity far exceeding the theoretical value is unreasonable. Furthermore, key mechanistic aspects, such as the dynamic interfacial behavior and the composition analysis of the interface, are insufficiently substantiated. These issues must be adequately addressed to support the conclusions.
1. The authors mention that multivalent states (HVOC) are superior to monovalent states (MVOC). Is this result specific to certain molecules, such as the target molecules described in the manuscript, or does it possess a certain degree of universality? Research review could easily reveal that some scholars have achieved similar effects for iodine cathode using monovalent cationic salts.
2. From a material perspective, the applicability of HVOC mentioned in this paper appears to be limited. First, the complexity of the synthesis process increases the cost of the product. Second, the authors do not provide the purity of the materials. The authors studied tetravalent cations, but how do by-products affect battery performance? There is no explanation regarding whether di- or trivalent cationic systems might form due to insufficient ionization during synthesis. Compared to other types of industrially accessible and low-cost additives, a novel but complex material may not offer strong advantages, whether as a poly-iodine absorbent or an anode protector.
3. The authors used Zn(OTF)2 to prepare the electrolyte. However, in aqueous iodine batteries, ZnSO4 seems to be gradually replacing such expensive salts. Have the authors investigated the battery behavior in ZnSO4 electrolyte?
4. The authors provide photos and UV-vis data of MVOC and HVOC adsorbing poly-iodine in Figure 1. Specific data analysis should be conducted to enhance the statement. Furthermore, the authors also present the cycling performance of high-loading batteries. Under high-loading conditions, the same HVOC concentration in the electrolyte should be affected by the sharp increase in iodine loading, which the authors need to explain.
5. On pages 8 and 9, the authors simulate the state of HVOC and the density of water at the anode/cathode interfaces in the discharged/charged states, respectively. However, it is necessary to consider whether the charged Zn anode and the discharged iodine cathode have the same effect. During the charging process, the cathode involves the transformation of iodide ions into poly-iodine. Would HVOC at the cathode migrate to the anode under the influence of the electric field? If so, what would be the state of the additive at the interface? Similarly, is the anode interface affected during the discharge process?
6. For the Raman tests, the authors chose to track the C-H stretching vibration band as the characteristic peak of HVOC. Are there other peaks, such as those related to N, that could also support the point? Secondly, the authors mention that the components of the anode interface layer are ZnSx/ZnFx. The changes in OTF- ions at the interface should also be considered.
7. The XPS results show that the amounts of ZnFx and ZnSx in the anode of the HVOC-added battery are greater than those in the BE electrolyte. What causes this? Additionally, the authors need to supplement and analyze the XPS of HVOC molecule and HVOC solely adsorbed with Ix- to provide a deeper explanation of the interface issues.
8. From the authors' visual adsorption tests, UV analysis, and Raman analysis, it is evident that HVOC has a strong interaction with polyiodines, almost preventing the dissolution of polyiodines (as seen in UV-vis and visible photos). However, in Figures S33 and S34, unavoidable capacity loss occurs during the initial activation (approximately from 270 to

200 mAh g-1 at 1A g-1). Moreover, the authors do not seem to mention the presence of iodine plus. The initial specific capacity in Figure S34 is 400 mAh g-1, which far exceeds the theoretical specific capacity (~211 mAh g-1) and is unreasonable (the authors mention that activated carbon contributes only 30 mAh g-1 at 1A g-1).
9. The schematic illustration in Figure 1 is complex, making it difficult to directly understand the scientific issue the authors intend to address or the innovation of this manuscript. It may fail to highlight the key scientific problem that needs to be communicated to readers.

Reviewer #2

(Remarks to the Author)
Review comments for “Tetravalent organic cation-enabled dual interfacial regulation for durable aqueous zinc–iodine batteries”:
Feng D. and Xu J. et al. proposed a high valent organic cation electrolyte additive (HVOC) to simultaneously regulate the interfacial properties of I2 cathode and Zn anode, achieveing stable cycling of Zn-I2 batteries. The MD simulation, in-situ Raman, XPS, TOF-SIMS were used to probe the interface of both electrodes. Good electrochemical performances of Zn||Zn, Zn||Cu and Zn||I2 cells were presented. However, there are substantial scientific and logic flaws in its current form, which is not suitable for publication on Nat Commun:
1. HVOC, solvation structure and water activity.
a. Why does HVOC ehnace Zn2+-OTF coordination? As a tetravalent cation, one would expect HVOC should coordinates with OTF over Zn2+.
b. Authors repeatedly mention that water activity is suppressed by HVOC. How does it exactly work? Please explain in detail. In addition, in-situ Raman at bond regions of water should be analyzed to show how water structure changes at the interface during cycling.
c. The schematical illustration of solvation structure in both electrolytes should be provided.
2. XPS, SEI and Zn plating kinetics
a. Why is there a N signal in BE electrolyte? There is no N-contained component in BE electrolyte if I understand it correctly
b. Usually, C 1s at 284.8 eV is set as reference, not 284.4 eV. The C1s fitting spectra should be provided
c. S 2p should be fit with 2p ½ and 2p 3/2. It is unprofessional and unscientific to fit S2p with one peak. Much more rigorous analysis is required for XPS fitting.
d. Authors repeatedly claim that ZnSx and ZnFx can enhance Zn deposition kinetics. Why? How does Zn2+ transport in ZnS and ZnF2? One would expect it will be slow in such inorganic components, especially for Zn2+ with two charges. The electrostatic force between Zn2+ and these inorganic frameworks should be strong. In fact, in Fig 5g, the overpotential of BE is even lower than that of HVOC-based electrolyte.
e. “This robust inorganic phase provides excellent electronic insulation and mechanical strength, effectively accommodating volume changes and relieving interfacial stress during repeated Zn plating/stripping.” Why? Please provide the evidence.
f. Authors mentioned that ZnFx/ZnSx SEI lowers the charge-transfer resistance, however, the Rct is actually higher in HVOC electrolyte in Fig S26.
3. For most of physical characterization and simulations, the exact electrolyte formula is missing. In addition, is Zn(OTf)2 concentration an important factor? 3m is a relatively high concentration. Does this strategy apply to more cost-friendly ZnSO4?
4. For CA analysis, please explain in detail or clearly label 2D vs. 3D contribution. Right now, it is confusing.
5. Fig 4i, why does a 0.997 r2 indicates the highly reversible redox process? The behind equations and logic should be presented in more detail.

Reviewer #3

(Remarks to the Author)
This work presents an innovative electrolyte design strategy using high-valence organic cations to regulate both the iodine cathode and Zn anode interfaces. The approach effectively mitigates polyiodide shuttle and Zn corrosion, delivering high capacity and stable cycling under various practical conditions. The underlying mechanisms have also been elucidated through detailed characterizations. With sufficient novelty in electrolyte design and clear performance improvement, this work should be of interest to researchers in the field. Therefore, I recommend its publication in Nature Communications after addressing the following concerns.

Below are the detailed concerns for the authors:
1. The discussion on EDL structures in different electrolyte systems is incomplete without considering the MVOC system. Simulation data for MVOC under the same electric field conditions as HVOC are necessary to convincingly highlight the advantages of HVOC.
2. Despite the HVOC-based electrolyte exhibiting lower desolvation energy compared to BE, it presents a higher overpotential in symmetrical cell tests. The authors should provide a detailed discussion to explain this phenomenon.
3. The authors claim that HVOC optimizes Zn nucleation morphology based on chronoamperometry measurements. It is recommended that additional experimental evidence, such as microscopic characterization, be provided. Such data would also help clarify how nucleation behavior influences interfacial stability and electrochemical performance.
4. Considering the effect of concentration polarization, the authors should include a comparison of Zn2+ diffusion coefficients in different electrolyte systems. This data would provide valuable insight into the mechanisms underlying the long-term cycling stability of Zn–I2 batteries.

5. At 5 A g–1, the HVOC-based Zn–I2 battery indeed shows longer cycling stability than BE and MVOC, which is encouraging. However, can this superiority be maintained at lower current densities (for example 0.2 A g–1). where side reactions are typically more pronounced.
6. The manuscript shows that HVOC improves Zn nucleation and deposition. However, its effect on Zn corrosion resistance is not examined. Given the corrosion issues in Zn–I2 batteries, could the authors provide relevant characterization and compare the HVOC-based electrolyte with BE and MVOC systems? Such analysis is important for assessing Zn anode stability and battery reversibility.
7. To improve the reproducibility of pouch cell performance, could the authors provide comprehensive and detailed information regarding the pouch cell assembly? It is recommended to include these details in Supplementary Information.

Version 1:

Reviewer comments:

Reviewer #1

(Remarks to the Author)
This study proposes the use of a high-valent organic cation (HVOC) to construct dual interfaces to improve the stability of Zn-I2 batteries, demonstrating promising performance. Although the authors have provided point-by-point responses to the concerns and addressed some related questions, in terms of innovation, this work still does not possess the potential for publication in Nature Communications. As a polyiodide adsorption system, it fails to raise a novel concept, and extensive literature already exists on cationic additives capable of adsorbing polyiodide ions (Adv. Energy Mater. 2024, 14, 2402306; Nat Commun 16, 4586 (2025); Energy Environ. Sci., 2025, 18, 4800-4810) and improving Zn anode deposition behavior (Adv. Mater. 2024, 36, 2408287. Adv. Energy Mater. 2022, 12, 2102780; J. Am. Chem. Soc. 2025, 147, 10, 8523–8533; J. Am. Chem. Soc., 2024, 146, 21377–21388). At its core, this research merely introduces a similar molecule, which is not irreplaceable. Furthermore, the revised manuscript has introduced new issues, and some existing problems remain inadequately substantiated:
1. The author list in the revised manuscript does not match that of the initial version, even resulting in the removal of a corresponding author. This is unreasonable for the lack of previous responsibility.
2. Regarding the purity of the material, the mass spectrometry (MS) results of HVOC provided by the authors are not considered sufficient proof of the purity. The authors did not provide liquid chromatography (LC)data; MS results can only confirm the presence of the target molecule. For material purity, a combination of 1H NMR, 13C NMR, or possibly 15N NMR would be more conclusive.
3. In the response file, the authors present R8 c (S64-c), which shows long-term cycling data of Zn–I2 batteries in different electrolytes. However, the figure indicates that using only ZnSO4 as the salt also enables relatively good cycling performance, remaining stable for 6000 cycles with high and stable Coulombic efficiency. There is no significant difference observed in the initial charge/discharge trends (0-200 cycles) and the subsequent prolonged cycling of base ZnSO4 and HVOC-containing electrolytes. How, then, is the specific role of the additive defined? Conversely, when the authors used Zn(OTF)2 as the salt, the blank electrolyte exhibited worse performance (Fig. 6b). Although the authors mention improved performance at low temperatures, the manuscript is clearly not focused on low-temperature systems

Reviewer #2

(Remarks to the Author)
The authors have addressed all my concerns. I appreciate authors' detailed and comprehensive answers, and glad to recommend this work for publication on Nat Commun.

Reviewer #3

(Remarks to the Author)
I have reviewed the response, all my concerns have been addressed properly. I have mo more questions.

Version 2:

Reviewer comments:

Reviewer #1

(Remarks to the Author)
The authors have addressed my concerns and improved the manuscript further.

Below please check for our **point-by-point responses to the reviewers' comments**, which are also incorporated into our revised manuscript.

Enumerated responses to comments from the reviewers.

Blue type: Reviewers' comments; **Black italic**: Our responses; Red type: Notable changes.

The corresponding update has been highlighted in Yellow in the revised manuscript.

Response to Reviewers

Reviewer #1:

This work proposes the use of a high-valent organic cation (HVOC) to construct dual interfaces for improving the stability of Zn–I_2 batteries, and the results demonstrate promising performance. However, several important issues need to be clarified. The synthesis of the HVOC molecule is complicated and costly, raising doubts about its practical applicability. On the experimental side, the use of $Zn(OTF)_2$ instead of more economical $ZnSO_4$ lacks justification, the rationale behind the HVOC concentration under high loading iodine is not explained, and the initial capacity far exceeding the theoretical value is unreasonable. Furthermore, key mechanistic aspects, such as the dynamic interfacial behavior and the composition analysis of the interface, are insufficiently substantiated. These issues must be adequately addressed to support the conclusions.

Response: We sincerely thank the reviewer's time and effort for evaluating our manuscript. In the revised version, we have specifically addressed the reviewer's concerns by clarifying that HVOC can be synthesized via a simple and scalable procedure, explaining our choice of $Zn(OTF)_2$ as the salt and further validating the applicability of the high-valent organic cation strategy in more cost-effective $ZnSO_4$-based electrolytes, carefully re-examining and rationalizing the reported capacity values, and strengthening the analysis of interfacial structure and dynamics. The following is the point-by-point response to all the questions. We hope you will find the revised manuscript has satisfactorily addressed your concerns.

Comments:

1. The authors mention that multivalent states (HVOC) are superior to monovalent states (MVOC). Is this result specific to certain molecules, such as the target molecules described in the manuscript, or does it possess a certain degree of universality? Research review could easily reveal that some scholars have achieved similar effects for iodine cathode using monovalent cationic salts.

Response: We appreciate the reviewer's insightful comment. We agree that monovalent cationic salts can effectively regulate iodine cathodes, as reported in previous studies, and our intention is to demonstrate that multivalent cations are one step further beyond monovalent. Multivalent cation strategy is not specific to the reported molecules in the manuscript. Rather, it can be extended to other molecules such as 1-methyl-1-propyl-pyrrolidinium bromide (Spy^{+}–Br), 1,1'- (propane-1,3-diyl) bis(1-methyl-pyrrolidinium) bromide (Dpy^{2+}–Br) as discussed in detail in the following section. Therefore, the additional benefit associated with higher cation valence within a comparable molecular scaffold, that is, to treat valence as a general design parameter. To place our results in context, we have also compiled a comparison of representative monovalent cation–based Zn–I_2 systems from the literature and our HVOC system (Table R1), which shows that the cycling stability and capacity retention achieved in this work are superior to those of reported monovalent cationic additives.

Table R1. A comparison of Zn–I_2 battery performance.

Modified strategies		**Z**	**I_2 loading (mg cm^{-2})**	**Cycling performance**	**Temperature (^{o}C)**	**Ref.**
HVOC-based	$OTF(OTF)_4$	**+4**	**2**	**99.9%@130 cycles**	**-40**	***This work***
			22	**97.2%@250 cycles**	**25**	
			17.1	**86.1@100 cycles**	**60**	
MVOC-based	TMAF	+1	1.5	~95.5%@250 cycles	30	[1]
	TMAI		15	91.3@100 cycles	25	[2]

	BmBr/ZSO	11.85	95.8@100 cycles	25	[3]
	PDDA-I	12.6	90.9@250 cycles	25	[4]

[1] *Nat. Commun.* 16, 4586 (2025)*;* [2] *Energy Environ. Sci.* 18, 4800-4810 (2025)*;* [3] *J. Am. Chem. Soc. 147, 8523-8533* (2025)*;* [4] *Angew. Chem. Int. Ed.* 64, e202510737 (2025).

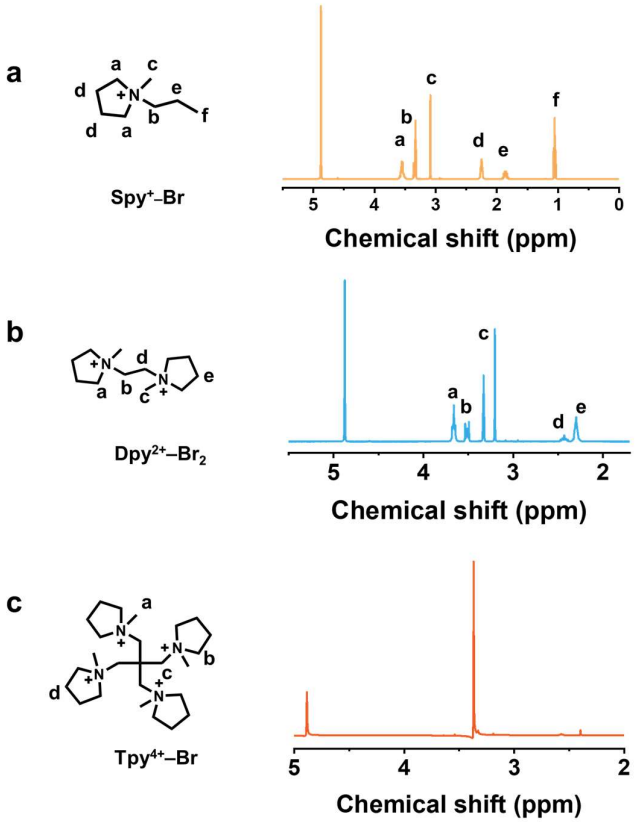

Fig. R1 Molecular structures and corresponding ^{1}H NMR spectra of **a** Spy^{+}, **b** Dpy^{2+}, and **c** Tpy^{4+}.

Beyond the specific HVOC used in the revised manuscript, we further synthesized a series of structurally related cations with different valence states, following literature procedures (*Angew. Chem. Int. Ed. 64, e202416092 (2024)*), namely 1-methyl-1-propyl-pyrrolidinium bromide (Spy^{+}–Br), 1,1'- (propane-1,3-diyl) bis(1-methyl-pyrrolidinium) bromide (Dpy^{2+}–Br), and 1,1'-(2,2-bis((1-methylpyrrolidinium-1-yl)methyl) propane-1,3-diyl)bis(1-methylpyrrolidinium) bromide (Tpy^{4+}–Br) (Fig. R1). NMR characterization confirms the successful synthesis of the Spy^{+}–Br and Dpy^{2+}–Br, whereas the Tpy^{4+}–Br could not be obtained despite multiple attempts. We therefore

focused on comparing Spy^{+} and Dpy^{2+} under identical conditions.

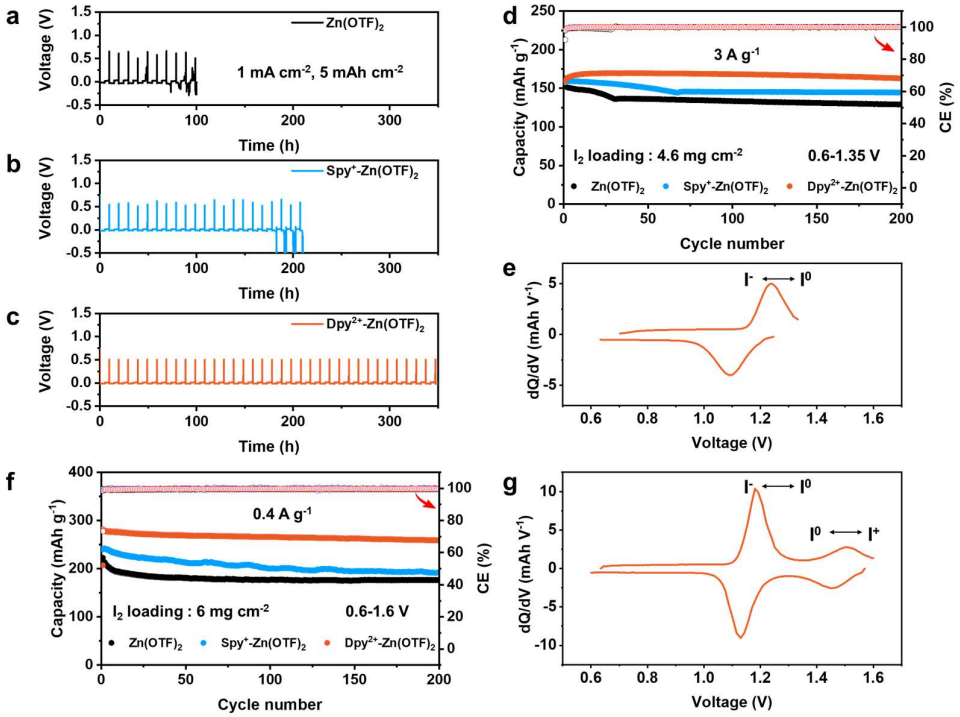

Fig. R2 Long-term cycling stability of Zn||Cu cells at 1 mA cm^{-2}, 5 mAh cm^{-2} with **a** $Zn(OTF)_2$, **b** Spy^{+}–$Zn(OTF)_2$, and **c** Dpy^{2+}–$Zn(OTF)_2$. **d** Cycling stability of Zn–I_2 battery with $Zn(OTF)_2$, Spy^{+}–$Zn(OTF)_2$, and Dpy^{2+}–$Zn(OTF)_2$ within 0.6-1.35 V. **e** dQ/dV curves of Zn–I_2 battery with Dpy^{2+}–$Zn(OTF)_2$ within 0.6-1.35 V. **f** Cycling stability of Zn–I_2 battery with $Zn(OTF)_2$, Spy^{+}–$Zn(OTF)_2$, and Dpy^{2+}–$Zn(OTF)_2$ within 0.6-1.6 V. **g** dQ/dV curves of Zn–I_2 battery with Dpy^{2+}–$Zn(OTF)_2$ within 0.6-1.6 V.

In 3 m $Zn(OTF)_2$ electrolytes with the same additive concentration, Zn||Cu cells were first used to evaluate Zn reversibility. At a current density of 1 mA cm^{-2} and an areal capacity of 5 mAh cm^{-2}, the cycling lifetime of Zn||Cu cells is extended from about 69 h in the bare $Zn(OTF)_2$ electrolyte to 178 h with Spy^{+} and 350 h with Dpy^{2+}, indicating that the higher-valent Dpy^{2+} more effectively stabilizes Zn plating/stripping (Figs. R2a-c). We then assembled Zn–I_2 full batteries with an iodine loading of 4.6 mg cm^{-2} and tested at a relatively high current density of 3 A g^{-1} for fast screening. A voltage window of 0.6–1.35 V was applied to exclude Br^{-}-induced I^0/I^+ and Br^{-}/Br^0 redox processes (*Adv. Mater. 37, e13389 (2025); Angew. Chem. Int. Ed. 63, e202403187 (2024)*). Under

these conditions, the Dpy^{2+}-containing electrolyte delivers improved cycling stability, with nearly 100% capacity retention after 200 cycles, compared with 92.8% for Spy^{+}-containing electrolyte and 86.0% for the bare $Zn(OTF)_2$ electrolyte (Fig. R2d). The corresponding dQ/dV profiles confirm that only the I^{-}/I^{0} redox couple is involved (Fig. R2e). It is found that the introduction of Br^{-} can successfully active I^{0}/I^{+} conversion under a wider voltage window of 0.6–1.6 V. At a relatively low current density of 0.4 A g^{-1}, the Dpy^{2+}-based electrolyte retains 92.7% of its capacity after 200 cycles, significantly outperforming Spy^{+}-containing electrolyte (80.0%) and the bare $Zn(OTF)_2$ electrolyte (79.3%) (Fig. R2f). As shown in Fig. R2g, Br^{-} can activate higher-valent iodine redox (I^{0}/I^{+}), which leads to capacities exceeding the theoretical value for the I^{-}/I^{0} (211 mAh g^{-1}). These results are consistent with our original conclusion that increasing cation valence enhances interfacial regulation and iodine redox reversibility.

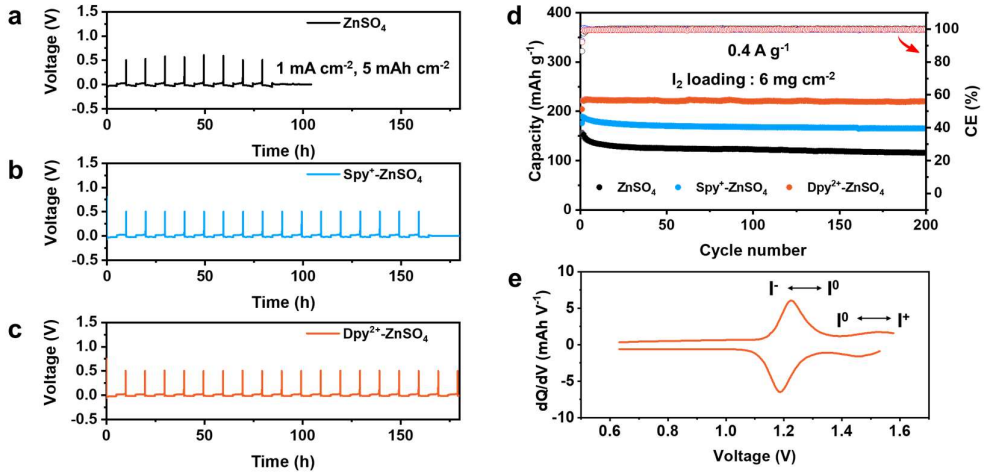

Fig. R3 Long-term cycling stability of Zn||Cu cells at 1 mA cm^{-2}, 5 mAh cm^{-2} with **a** $ZnSO_4$, **b** Spy^{+}–$ZnSO_4$, and **c** Dpy^{2+}–$ZnSO_4$ electrolytes. **d** Cycling stability of Zn–I_2 battery with $ZnSO_4$, Spy^{+}–$ZnSO_4$, and Dpy^{2+}–$ZnSO_4$ electrolytes within 0.6-1.6 V. **e** dQ/dV curves of Zn–I_2 battery with Dpy^{2+}–$ZnSO_4$ electrolyte within 0.6-1.6 V.

To further assess the generality of this valence effect in more practical electrolytes, we also tested $ZnSO_4$-based systems with equal amounts of Spy^{+} and Dpy^{2+}. Both cations improve Zn reversibility compared with bare $ZnSO_4$, and Dpy^{2+} again provides higher capacity and better cycling stability in Zn–I_2 full cells than Spy^{+} (Fig. R3), supporting the conclusion that multivalent cations offer a stronger interfacial regulation

effect than their monovalent analogues within the same structural framework. These additional results indicate that the superiority of multivalent cations is not limited to the specific HVOC molecule originally studied, but rather demonstrates a certain degree of universality that can be extended to other organic cation systems and to more cost-effective $ZnSO_4$ electrolytes. The corresponding data and discussion have been added to the revised Supplementary Information (Supplementary Figs. 66-68) and revised manuscript (Page 24).

2. From a material perspective, the applicability of HVOC mentioned in this paper appears to be limited. First, the complexity of the synthesis process increases the cost of the product. Second, the authors do not provide the purity of the materials. The authors studied tetravalent cations, but how do by-products affect battery performance? There is no explanation regarding whether di- or trivalent cationic systems might form due to insufficient ionization during synthesis. Compared to other types of industrially accessible and low-cost additives, a novel but complex material may not offer strong advantages, whether as a poly-iodine absorbent or an anode protector.

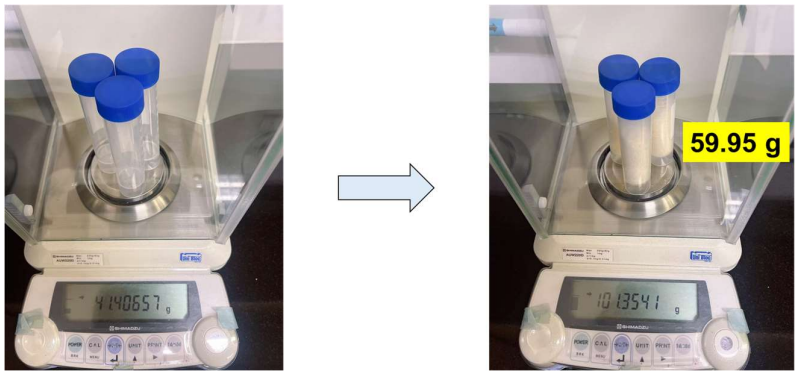

Fig. R4 Photograph of batch-prepared HVOC-containing $OTA(OTF)_4$.

Response: We thank the reviewer for these important and very practical comments. Regarding synthetic complexity and cost, HVOC-containing $OTA(OTF)_4$ is prepared by reacting two low-cost, commercially available precursors (0.57$/g for 1,4,7,10-Tetraazacyclododecane and 0.046$/g for Allyl bromide from https://www.aladdin-e.com/) in acetonitrile under reflux, followed by a simple ion-exchange step. Both steps are standard operations in organic salt synthesis and do not require metal catalysts, inert

atmosphere protection, or multistep chromatographic purification. As shown in Fig. R4, this procedure can be readily scaled to batch quantities of several tens of grams in our laboratory (e.g. 59.95 g). Compared with many reported organic additives that rely on expensive starting materials, precise stoichiometry control, protected atmosphere, and repeated purification to obtain only gram-scale quantities, the present route is relatively simple and cost-effective. We also expect that further optimization of catalyst, solvent, and reaction temperature could reduce the time and energy cost, although a complete techno-economic analysis is beyond the scope of this work.

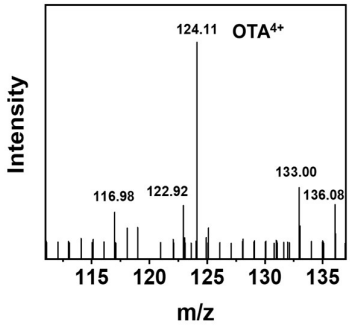

Fig. R5 High-resolution mass spectrometry for $OTA(OTF)_4$.

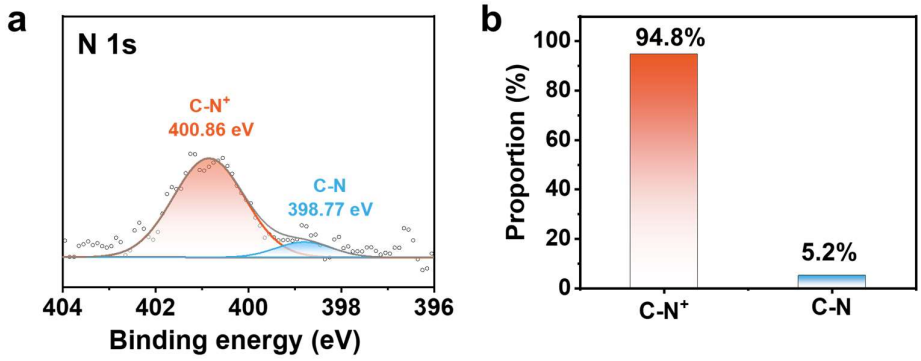

Fig. R6 **a** N 1s XPS patterns of $OTA(OTF)_4$ and **b** the corresponding calculated proportion of $C–N^+$ and C–N components.

Regarding the purity and possible by-products, we have added explicit characterization data in the revised manuscript. High-resolution mass spectrometry (HRMS) shows a dominant signal at m/z = 124.11 (Fig. R5), attributable to the targeted tetravalent cation and fully consistent with the synthesis reported in the literature that

we referred (*Energy Environ. Sci. 17, 4519 (2024)*). The ^{1}H NMR spectra (Supplementary Fig. 3) also match the reported data, indicating high molecular purity. However, high-resolution N 1s XPS reveals a small contribution from C–N (5.2%) alongside C–N^{+} (94.8%), suggesting that a trace amount of unquaternized precursor cannot be completely excluded (Fig. R6). This implies that minor di- or trivalent species may exist at a low content, and their potential influence on the electrochemical response cannot yet be fully ruled out. Nevertheless, this does not affect our central conclusion that higher-valent organic cations outperform monovalent ones. As shown in Figs. R1-R3, their electrochemical performance follows the trend Dpy^{2+} > Spy^{+} under identical conditions, fully consistent with our original conclusion that higher valence is beneficial. Moreover, previous studies on electrolytes for Li-metal batteries have independently reported a similar sequence of electrochemical performance, namely tetravalent > divalent > monovalent cations (*Angew. Chem. Int. Ed. 64, e202416092 (2024)*), which further supports the reliability of our interpretation. The corresponding data and discussion have been added to the revised Supplementary Information (Supplementary Figs. 4-6) and main text in the revised manuscript (Page 6).

We also fully agree with the reviewer that, from an industrial standpoint, simple, low-cost additives are required. Our primary aim in this work is therefore to establish and validate a high-valent organic cation strategy for dual interfacial regulation, rather than to position the present $OTA(OTF)_4$ as the only practical candidate. The additional Dpy^{2+} in $ZnSO_4$-based results show that this high-valent organic cation strategy is not limited to a specific cation and can be realized with simpler and more economical cationic species.

3. The authors used $Zn(OTF)_2$ to prepare the electrolyte. However, in aqueous iodine batteries, $ZnSO_4$ seems to be gradually replacing such expensive salts. Have the authors investigated the battery behavior in $ZnSO_4$ electrolyte?

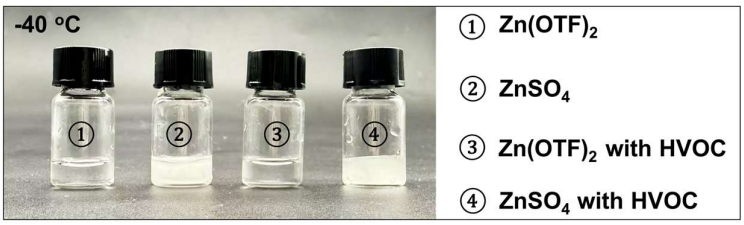

Fig. R7 Optical photographs of different electrolytes at −40 °C.

Response: We appreciate the reviewer's insightful comment on the electrolyte selection. We acknowledge that $ZnSO_4$ possesses clear advantages in terms of cost and accessibility compared with $Zn(OTF)_2$. However, the choice of $Zn(OTF)_2$ in this work was based on two essential considerations: (1) Temperature adaptability. According to the Hofmeister series (*Adv. Mater. 34, 2110140 (2022)*), the chaotropic OTF^- disrupts the hydrogen-bond network of water more strongly than the kosmotropic SO_4^{2-} anion, which endows OTF^--based electrolytes with superior antifreezing ability. This property is critical for achieving low-temperature operation of aqueous batteries. As displayed in Fig. R7, the $Zn(OTF)_2$-based electrolyte containing HVOC remains unfrozen down to −40 °C, while the $ZnSO_4$-based counterpart freezes, highlighting the advantage of OTF^- anions in depressing the freezing point and enhancing low-temperature adaptability. (2) Interface protection and SEI chemistry. $Zn(OTF)_2$ is also well recognized for its ability to facilitate the formation of ZnF_x/ZnS_x-rich interfacial layers (*Nat. Nanotechnol. 16, 902-910 (2021); Angew. Chem. Int. Ed. 62, e202302583 (2023); Matter 7, 4014-4030, (2024); Joule 9, 101844, (2025) and et al*), which exhibit high ionic transport and effectively suppress parasitic reactions such as hydrogen evolution and polyiodide-induced corrosion in aqueous iodine batteries.

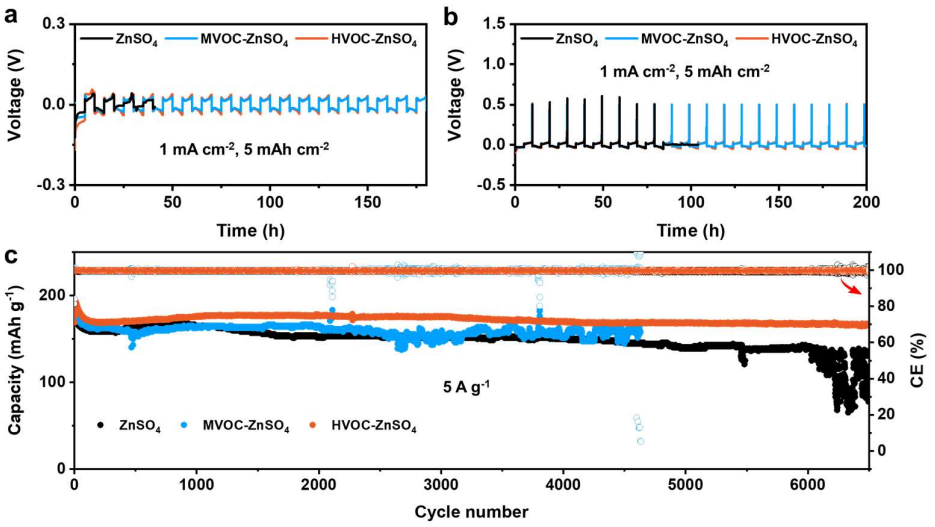

Fig. R8 a Long-term cycling stability of Zn||Zn cells at 1 mA cm^{-2}, 5 mAh cm^{-2} with HVOC in $ZnSO_4$-based electrolytes. **b** Long-term cycling stability of Zn||Cu cells at 1 mA cm^{-2}, 5 mA h cm^{-2} with HVOC in $ZnSO_4$-based electrolytes. **c** Cycling stability of Zn–I_2 battery with HVOC in $ZnSO_4$-based electrolytes.

To assess the broader applicability of the high-valent organic cation strategy, we further evaluated $ZnSO_4$-based electrolytes containing MVOC or HVOC with the same concentration. At a current density of 1 mA cm^{-2} with an area capacity of 5 mAh cm^{-2}, Zn||Zn and Zn||Cu cells using MVOC- or HVOC-containing $ZnSO_4$-based electrolytes exhibit markedly improved Zn reversibility compared with the $ZnSO_4$ (Figs. R8a and b). The increased overpotential observed in HVOC-containing $ZnSO_4$-based electrolyte is associated with interfacial electrostatic shielding or competitive adsorption induced by high-valent cations at the Zn surface (*Nat. Commun. 13, 3252 (2022); Energy Environ. Sci. 16, 4561 (2023)*). In full Zn–I_2 batteries, the HVOC-containing $ZnSO_4$ electrolyte delivers superior cycling stability and stable Coulombic efficiency (CE), outperforming not only the bare $ZnSO_4$ electrolyte but also the MVOC-containing system (Fig. R8c). These results demonstrate that the high-valent organic cation strategy is not limited to $Zn(OTF)_2$ and can also be applied in more cost-effective $ZnSO_4$-based electrolytes. The corresponding data and discussion have been added to the revised Supplementary Information (Supplementary Figs. 64-65) and revised

manuscript (Page 24).

4. The authors provide photos and UV-vis data of MVOC and HVOC adsorbing poly-iodine in Figure 1. Specific data analysis should be conducted to enhance the statement. Furthermore, the authors also present the cycling performance of high-loading batteries. Under high-loading conditions, the same HVOC concentration in the electrolyte should be affected by the sharp increase in iodine loading, which the authors need to explain.

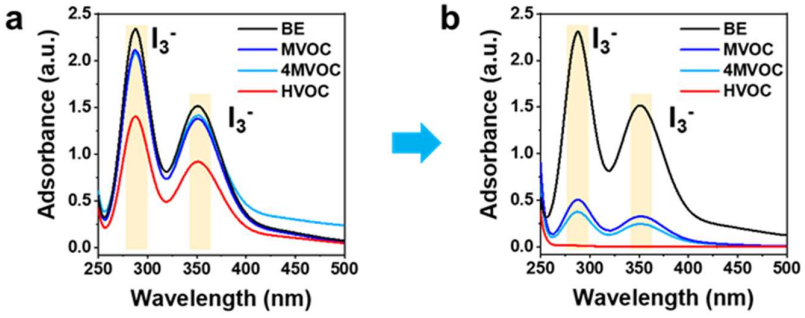

Fig. R9 UV–Vis absorption spectra of polyiodide retention experiments in various electrolytes **a** at 0 h and **b** after 12 h.

Response: We appreciate the reviewer's valuable suggestion. To strengthen the quantitative validity of the visual and UV–Vis evidence in Fig. 1, we conducted additional comparative analyses of the characteristic I_3^- absorption peaks at 287.9 nm and 351.4 nm in different electrolyte systems. As shown in Fig. R9, the UV–Vis spectra before and after 12 h of standing were carefully compared. In BE, the absorption intensity of I_3^- remained essentially unchanged, indicating its high solubility of poly-iodine. When MVOC and 4MVOC were introduced, the absorbance decreased to approximately 24.3% and 17.3% of its original value, respectively. By contrast, the HVOC-containing electrolyte nearly eliminated the I_3^- absorption bands, demonstrating a much stronger capability to immobilize polyiodide species.

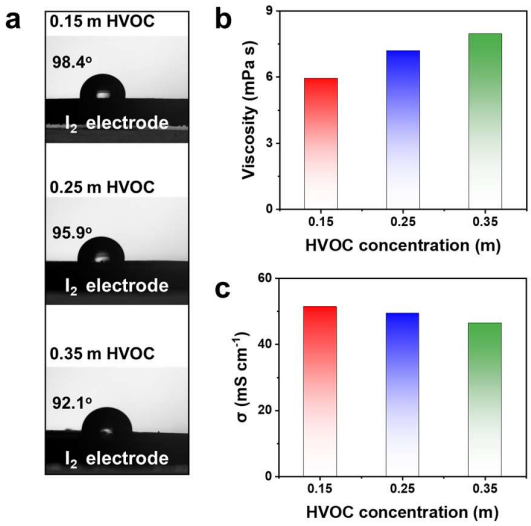

Fig. R10 a Contact angle of electrolytes with different HVOC concentration on I_2 electrode surface. **b** Viscosities and **c** Ionic conductivities of electrolytes with different HVOC concentrations.

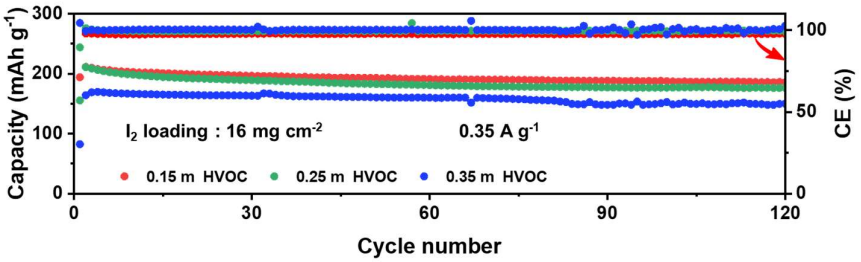

Fig. R11 Cycling stability of Zn–I_2 battery using electrolytes with different HVOC concentrations.

We also appreciate the reviewer's comment on whether the selected HVOC concentration remains appropriate under high iodine loading. The ability of HVOC to maintain effective polyiodide suppression at relatively low dosage arises from the intrinsically high charge density of the tetravalent cation, which enhances electrostatic association with polyiodide species and the iodine cathode surface. As a result, robust confinement is maintained even at a high iodine loading of 22 mg cm^{-2}, as reflected in the full-cell performance shown in Fig. 6d of the manuscript. In addition, the optimized HVOC concentration is not solely dictated by cathode side regulation, but is also constrained by Zn deposition reversibility. Systematical Zn||Cu performance

(Supplementary Fig. 50) identifies 0.15 m HVOC as the optimal concentration, that yields the longest Zn plating/stripping lifetime. Further increasing HVOC concentration results in degraded Zn reversibility, which is likely associated with excessive interfacial electrostatic shielding. Excessive shielding hinders Zn^{2+} transport and reduces kinetics.

Under high iodine loading conditions, interfacial wettability and bulk transport must also be balanced. Contact-angle measurements show that an appropriate amount of HVOC improves wetting of the I_2 cathode (Fig. R10a), whereas higher HVOC concentrations increase electrolyte viscosity and reduce ionic conductivity (Figs. R10b and c). Consistently, high-loading Zn–I_2 full cells (~16 mg cm^{-2}) show that 0.15 m HVOC-containing electrolyte delivers the best cycling performance (Fig. R11). These results confirm that the chosen HVOC concentration represents an optimized compromise among polyiodide immobilization, Zn deposition reversibility, and electrolyte transport properties under high-loading conditions. The corresponding data and discussion have been added to the revised Supplementary Information (Supplementary Figs. 11 and 60-61) and revised manuscript (Pages 7-8 and 23).

5. On pages 8 and 9, the authors simulate the state of HVOC and the density of water at the anode/cathode interfaces in the discharged/charged states, respectively. However, it is necessary to consider whether the charged Zn anode and the discharged iodine cathode have the same effect. During the charging process, the cathode involves the transformation of iodide ions into poly-iodine. Would HVOC at the cathode migrate to the anode under the influence of the electric field? If so, what would be the state of the additive at the interface? Similarly, is the anode interface affected during the discharge process?

Response: We thank the reviewers for these important comments. To strengthen the analysis of interfacial behavior, we expanded our simulations from a single-electrode configuration to a full-cell molecular dynamics (MD) model in which both electrodes were polarized simultaneously in BE, MVOC, and HVOC systems. This framework enables quantitative assessment of ion and solvent distributions under the coupled

electric fields characteristic of discharge and charge, thereby providing a more quantitative description of the interfacial structure at both electrodes.

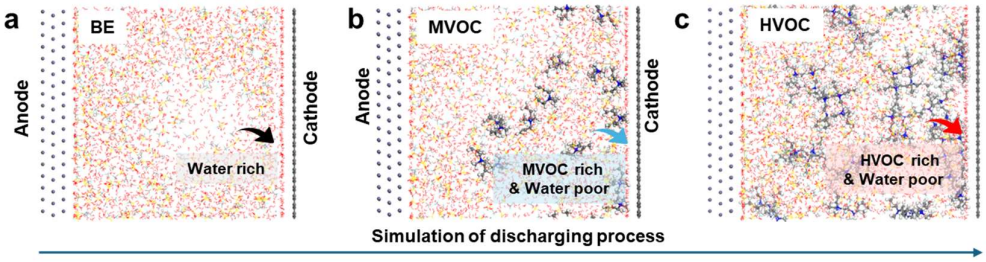

Fig. R12 MD simulated EDL configuration near the I_2 cathode and Zn anode with **a** BE, **b** MVOC and **c** HVOC during discharging.

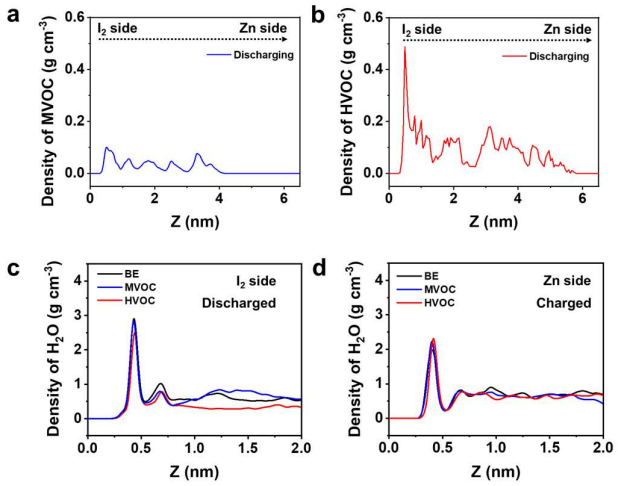

Fig. R13 **a** Corresponding cumulated density distributions of MVOC in MVOC electrolyte. **b** Corresponding cumulated density distributions of HVOC in HVOC electrolyte. **c** Corresponding cumulated density distributions of water molecules near discharged I_2 cathode in different electrolytes. **d** Corresponding cumulated density distributions of water molecules near charged Zn anode in different electrolytes.

As shown in Fig. R12a, the BE electrolyte forms a water-rich interfacial layer at the iodine cathode during discharge. These interfacial water molecules are highly reactive and facilitate the dissolution of polyiodide species and I_2, giving rise to pronounced shuttle effects and rapid capacity decay. In contrast, MVOC and HVOC-containing electrolytes exhibit distinct interfacial structures under the same conditions. Driven by the applied electric field, MVOC or HVOC molecules migrate toward the cathode, forming cation-enriched and water-deficient interfacial layers (Figs. R12b and R12c).

The corresponding ion distribution profiles (Figs. R13a and R13b) corroborate this interfacial enrichment, while the water density profiles (Fig. R13c) further show that HVOC achieves the most pronounced suppression of interfacial water.

For the charging state at the Zn anode, the reviewers' concerns were directly examined. In BE, the absence of cationic species leads to persistently water-rich interfaces at both the cathode and anode (Fig. R12a). In the MVOC system, the lower charge density of MVOC results in substantial field-driven migration toward the I_2 electrode, leaving negligible interfacial coverage at the Zn anode (Figs. R12b and R13a). In contrast, HVOC maintains a measurable interfacial presence at the Zn anode, which increases the separation between water molecules and the electrode compared with BE and MVOC (Figs. R12c, R13b and d).

To further analyze the evolution of the interfaces across different electrochemical states, we reversed the field polarity to simulate the transition from discharge to charge (Fig. R14). In BE, the interfacial environment remains water-rich at both electrodes (Figs. R14a and d). For MVOC and HVOC (Figs. R14b-f), the simulations reveal that HVOC remains partially accumulated at the iodine cathode during charging, thereby suppressing undesired side reactions. At the same time, both MVOC and HVOC migrate toward the Zn anode and form cation-enriched layers that increase the separation between water molecules and the electrode surface.

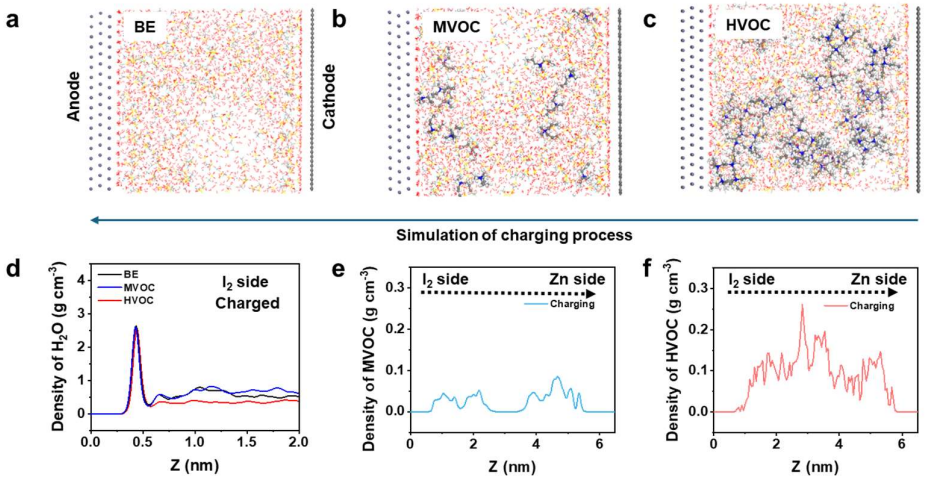

Fig. R14 MD simulated EDL configuration near the I_2 cathode and Zn anode with **a** BE, **b** MVOC and **c** HVOC during charging. **d** Corresponding cumulated density

distributions of water molecules near the charged I_2 cathode in different electrolytes. **e** Corresponding cumulated density distributions of MVOC in MVOC electrolyte. **f** Corresponding cumulated density distributions of HVOC in HVOC electrolyte.

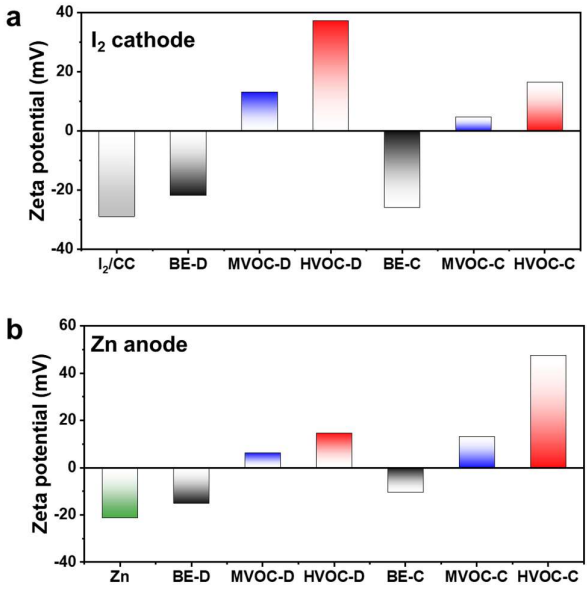

Fig. R15 Zeta potentials of the **a** discharged (D) and charged (C) I_2 cathode, and **b** discharged (D) and charged (C) Zn anode, comparing different electrolytes.

To experimentally validate this coupled interfacial behavior, we performed zeta potential measurements on both electrodes retrieved at discharged (0.6 V, D) and charged (1.8 V, C) states of the cycled batteries. As shown in Fig. R15, electrodes cycled in the presence of HVOC exhibit more positive zeta potential than those in BE or MVOC. Although the zeta potential of the charged I_2 cathode and discharged Zn anode are lower than those of their corresponding counter-states, both remain higher than the initial electrode values, and the HVOC-based electrodes consistently show the highest zeta potential among three systems. Additionally, XPS and TOF-SIMS analyses of the cycled electrodes reveal the presence of HVOC-derived species at both cathode and anode interfaces, confirming the formation of a persistent cationic interphase. We have revised the manuscript to include the full-cell interfacial analysis, zeta potential data, and supporting spectroscopic evidence to provide a more complete description of the interfacial behavior. The corresponding data and discussion have been added to the revised Supplementary Information (Supplementary Figs. 13-15 and 18) and revised

manuscript (Pages 8-10 and Figs. 2a-d).

6. For the Raman tests, the authors chose to track the C-H stretching vibration band as the characteristic peak of HVOC. Are there other peaks, such as those related to N, that could also support the point? Secondly, the authors mention that the components of the anode interface layer are ZnS_x/ZnF_x. The changes in OTF^- ions at the interface should also be considered.

Response: We sincerely thank the reviewer for this insightful comment. Before conducting the in-situ Raman measurements, we first compared the Raman spectra of BE and electrolytes containing different concentrations of HVOC (Supplementary Fig. 17). We found that, relative to BE, the C–H stretching vibration of HVOC shows a particularly clear and concentration-dependent change, with minimal spectral interference from other electrolyte components. This clear response is the main reason we chose the C–H band as the characteristic peak to monitor HVOC adsorption at the electrode/electrolyte interface. By contrast, under our electrolyte conditions, many of the remaining HVOC vibrational modes (including N-associated modes) overlap significantly with the intense Raman bands of $Zn(OTF)_2$ and water, which makes them unsuitable for reliable in-situ tracking. This spectral congestion limits the practical use of N-related peaks for dynamic interfacial analysis. To further support the conclusion that HVOC redistributes and adsorbs at the Zn interface, we additionally analyzed the evolution of interfacial water during Zn plating.

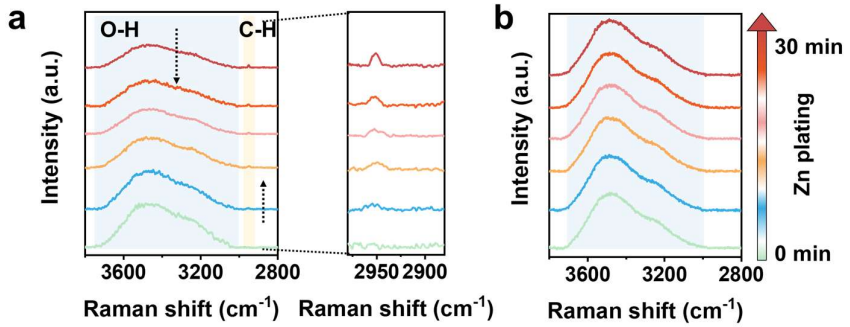

Fig. R16 In-situ Raman spectra in the range of 2800-3800 cm^{-1} of the Zn||Zn symmetrical cells with **a** HVOC and **b** BE during Zn plating.

As Fig. R16 shows, the broad band at 3000–3700 cm^{-1} corresponds to the O–H stretching vibration of water molecules. During Zn plating, the O–H intensity decreases markedly, coinciding with the increase in the HVOC-related C–H signal. This indicates that HVOC adsorption occupies interfacial sites, thereby reducing the number of water molecules at the Zn interface. In contrast, in BE, the O–H band remains consistently strong throughout the Zn plating, reflecting a persistently water-rich environment in the absence of HVOC. This complementary analysis of interfacial water evolution provides additional evidence for the interfacial adsorption of HVOC.

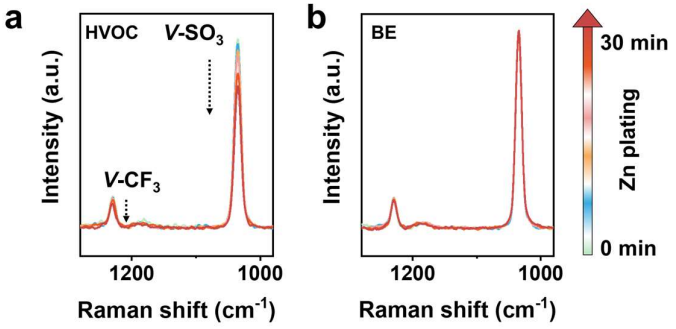

Fig. R17 In-situ Raman spectra in the range of 980-1280 cm^{-1} of the Zn||Zn symmetrical cells with **a** HVOC and **b** BE during Zn plating.

We also monitored the interfacial evolution of OTF^- during Zn plating by in-situ Raman spectroscopy. The bands at 1035.5 cm^{-1} and 1229.5 cm^{-1} are assigned to the ν-SO_3 and ν-CF_3 vibrations of OTF^-, respectively. During plating in the HVOC-containing electrolyte, the intensities of both peaks gradually decrease (Fig. R17a), indicating progressive decomposition of OTF^- to form the SEI. In contrast, only a slight decrease of these signals was observed in BE during the same time period (Fig. R17b). This suggests that more extensive OTF^- decomposition occurs at the interface in the HVOC system, contributing to the formation of ZnF_x and ZnS_x-rich inorganic SEI. This observation is consistent with the higher fraction of contact ion pairs (CIP) and aggregates (AGG) in the HVOC electrolyte, as evidenced by Raman analysis and MD calculations (Fig. R18). The corresponding data and discussion have been added to the revised Supplementary Information (Supplementary Figs. 39 and 43) and revised manuscript (Pages 17-18).

7. The XPS results show that the amounts of ZnF_x and ZnS_x in the anode of the HVOC-added battery are greater than those in the BE electrolyte. What causes this? Additionally, the authors need to supplement and analyze the XPS of HVOC molecule and HVOC solely adsorbed with I_x^- to provide a deeper explanation of the interface issues.

Response: We thank the reviewer for this thoughtful question. The higher amounts of ZnF_x and ZnS_x detected at the Zn anode in the HVOC-containing electrolyte mainly originate from a HVOC-induced reconfiguration of the Zn^{2+} solvation environment, which promotes OTF^--driven interfacial reduction, as demonstrated by MD and EXAFS analyses in the revised manuscript (Figs. 2i and j).

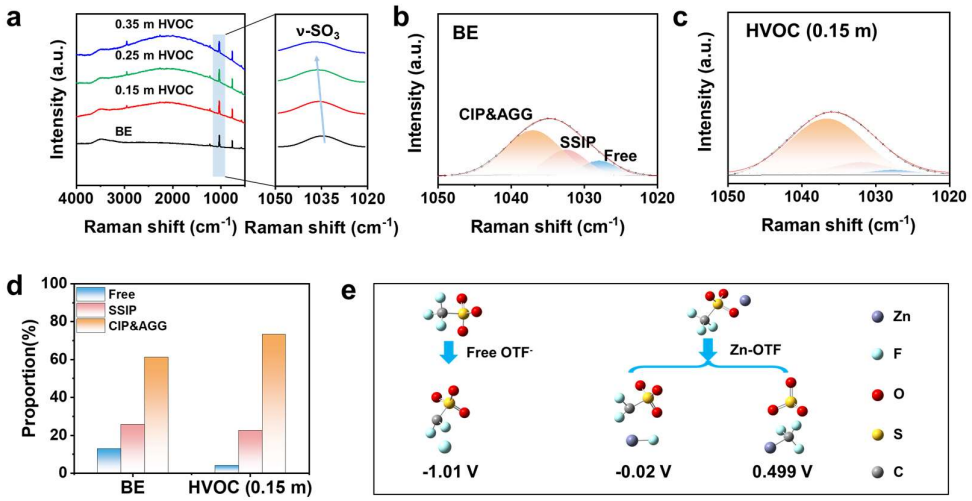

Fig. R18 a Raman spectra of BE and electrolytes with different concentrations of HVOC. The fitted Raman spectra of **b** BE and **c** HVOC (0.15 m). **d** The calculated free anion, SSIP and CIP&AGG area ratios. **e** Calculated reduction potentials by DFT.

To further substantiate this mechanistic interpretation, we performed additional Raman analyses of OTF^- coordination. In the 1020–1050 cm^{-1} region associated with the ν-SO_3 stretching of OTF^-, peak deconvolution allows us to distinguish free OTF^- (~1028 cm^{-1}), solvent-separated ion pairs (SSIP, ~1032 cm^{-1}), contact ion pairs and aggregates (CIP&AGG, ~1037 cm^{-1}) (*Energy Environ. Sci. 17, 9244 (2024)*). Increasing the HVOC concentration leads to a shift of the ν-SO_3 band toward higher wavenumbers (Fig. R18a) and an increase in the fractions of CIP and AGG species

(Figs. R18b-d), indicating more Zn^{2+}–OTF^{-} coordination. Complementary theoretical calculations show that OTF^{-} coordinated to Zn^{2+} exhibits an elevated reduction potential relative to free OTF^{-}, indicating that Zn^{2+}–OTF^{-} structures are more susceptible to reductive decomposition (Fig. R18e) (*Nat. Commun. 10, 5374 (2019); Adv. Funct. Mater. DOI: 10.1002/adfm.202523560 (2025)*). This trend is consistent with the greater abundance of ZnF_x and ZnS_x observed by XPS and TOF-SIMS.

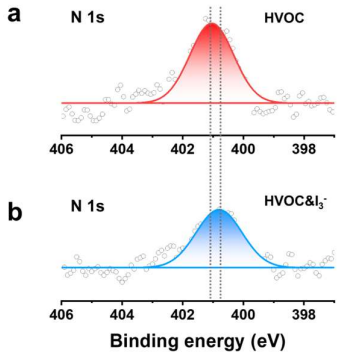

Fig. R19 N 1s XPS patterns of **a** HVOC and **b** HVOC&@ I_3^-.

Regarding the second point, we have supplemented the revised manuscript with XPS data for HVOC and HVOC&@ I_3^- (Fig. R19). In HVOC&@ I_3^-, the N 1s shifts to lower binding energy, attributable to partial charge transfer from iodide to the nitrogen-containing sites (*J. Am. Chem. Soc. 146, 6628-6637 (2024)*). This behavior further supports strong electrostatic and electronic interaction between HVOC and polyiodide species at the iodine cathode interface. The corresponding data and discussion have been added to the revised Supplementary Information (Supplementary Figs. 12, 23 and 24) and revised manuscript (Pages 8 and 11).

8. From the authors' visual adsorption tests, UV analysis, and Raman analysis, it is evident that HVOC has a strong interaction with polyiodines, almost preventing the dissolution of polyiodines (as seen in UV-vis and visible photos). However, in Figures S33 and S34, unavoidable capacity loss occurs during the initial activation (approximately from 270 to 200 mAh g^{-1} at 1A g^{-1}). Moreover, the authors do not seem

to mention the presence of iodine plus. The initial specific capacity in Figure S34 is 400 mAh g^{-1}, which far exceeds the theoretical specific capacity (~211 mAh g^{-1}) and is unreasonable (the authors mention that activated carbon contributes only 30 mAh g^{-1} at 1A g^{-1}).

Response: We sincerely thank the reviewer for the careful evaluation and constructive comments. We address each point in detail below.

(i) On the possible involvement of iodine-plus species.

We would like to clarify that the HVOC-based electrolyte operates exclusively through the I^-/I^0 redox couple. Cyclic voltammetry (Supplementary Fig. 37) shows no additional oxidative features attributable to I^+ species, confirming that iodine-plus chemistry is not involved in our system.

(ii) On the origin of the initial capacity decay.

The observed initial capacity decay is not caused by polyiodide dissolution. Instead, it arises from the capacitive contribution of the YP50 carbon host at low iodine loading. As shown in Supplementary Fig. S55, YP50 delivers 27.2 mA h g^{-1} at 1 A g^{-1} (YP50 loading: 7.5 mg cm^{-2}). When normalized to the iodine mass used in Supplementary Fig. S33 (2.3 mg cm^{-2}), this corresponds to ~88.6 mA h g^{-1}, which elevates the apparent initial capacity above the theoretical iodine capacity (211 mA h g^{-1}). A similar phenomenon has also been reported and rationalized in *J. Am. Chem. Soc. 146, 21377-21388 (2024)*. During the initial activation, the progressive adsorption of electrolyte cations onto carbon reduces the accessible surface area and diminishes the capacitive contribution, resulting in the observed initial capacity decay. A similar trend appears in low-loading long-cycle tests (Fig. 6b, I_2 loading is 2 mg cm^{-2}). Importantly, this effect disappears in high-loading batteries, as the capacity contribution of carbon becomes negligible. No abnormal initial capacity decay is observed in high-loading batteries (Figs. 6c, 6d, 6f, and Supplementary Fig. 63), confirming that the decline is unrelated to polyiodide dissolution.

(iii). On the incorrect initial capacity (~400 mA h g^{-1}) in Figure S34 (revised Supplementary Fig. 58).

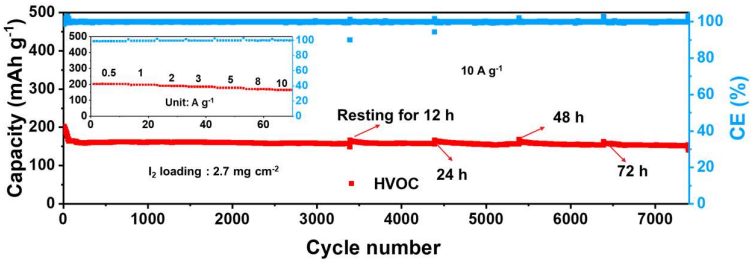

Fig. R20 Cycling stability of Zn–I_2 battery with HVOC electrolyte after different resting times at 10 A g^{-1}.

The abnormally high initial capacity in the earlier version of Fig. S34 (revised Supplementary Fig. 58) was caused by a data-export error in the Neware software. Specifically, the data were exported using the software's default cycle-integration mode, which incorrectly added the discharge capacity of the last cycle at one current density to the discharge capacity of the first cycle at the next current density. For example, the final discharge capacity at 0.2 A g^{-1} and the first discharge capacity at 0.5 A g^{-1} were inadvertently summed, producing an unrealistic value of 401.6 mA h g^{-1}. After correcting the data-export mode, this artifact disappeared (Fig. R20). We have now re-exported all rate-performance data according to the actual discharge–charge sequence and replaced the incorrect figure with the corrected one (Supplementary Fig. 58). In addition, we have carefully re-checked the entire dataset to ensure that no similar inconsistencies remain in the revised manuscript.

9. The schematic illustration in Figure 1 is complex, making it difficult to directly understand the scientific issue the authors intend to address or the innovation of this manuscript. It may fail to highlight the key scientific problem that needs to be communicated to readers.

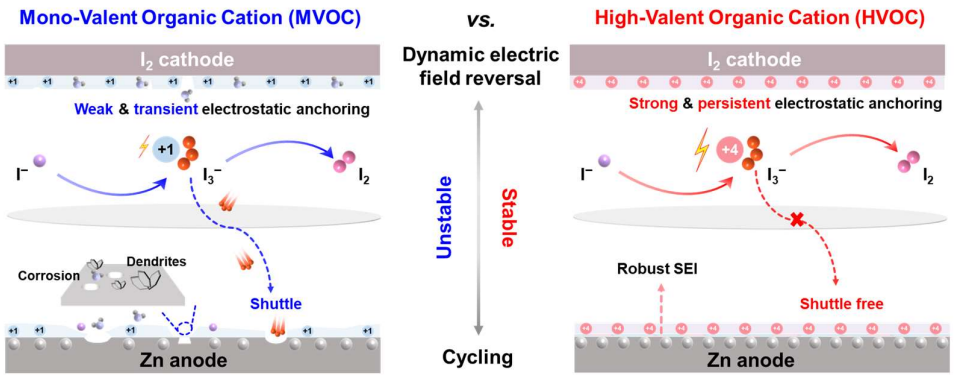

Fig. R21 The revised scheme 1.

Response: We appreciate the reviewer's constructive comment. In the revised manuscript, we have substantially simplified scheme 1, as shown in Fig. R21. Non-essential graphical elements have been removed and the annotations have been streamlined so that the figure can more directly convey the main scientific problem and the core innovation of this work. The updated schematic has replaced the original scheme 1 in the revised manuscript (Page 5).

Reviewer #2:

Review comments for "Tetravalent organic cation-enabled dual interfacial regulation for durable aqueous zinc–iodine batteries":Feng D. and Xu J. et al. proposed a high valent organic cation electrolyte additive (HVOC) to simultaneously regulate the interfacial properties of I_2 cathode and Zn anode, achieveing stable cycling of Zn-I_2 batteries. The MD simulation, in-situ Raman, XPS, TOF-SIMS were used to probe the interface of both electrodes. Good electrochemical performances of Zn||Zn, Zn||Cu and Zn||I_2 cells were presented. However, there are substantial scientific and logic flaws in its current form, which is not suitable for publication on Nat Commun:

Response: We sincerely appreciate the reviewer's critical and constructive comments, which have greatly helped us improve the clarity and rigor of our manuscript. In response, we have carefully revised the text (all changes highlighted in yellow), strengthened the mechanistic framework, and incorporated additional simulations and electrochemical analyses to address the raised concerns. Detailed point-by-point responses and supporting data are provided below. We truly hope that these revisions

adequately address your concerns.

1. HVOC, solvation structure and water activity.

a. Why does HVOC enhnace Zn^{2+}-OTF coordination? As a tetravalent cation, one would expect HVOC should coordinates with OTF over Zn^{2+}.

Response: We appreciate the reviewer's insightful question. To clarify the origin of the enhanced Zn^{2+}–OTF^{-} coordination, we carried out additional DFT calculations comparing the interaction of OTF^{-} with Zn^{2+} and with OTA^{4+} (HVOC). The calculated binding energy of the Zn^{2+}–OTF^{-} is larger that of the OTA^{4+}–OTF^{-}, indicating that OTF^{-} preferentially coordinates with Zn^{2+} rather than with HVOC (Fig. R22a). This preference can be understood by considering ionic size and steric factors. OTF^{-} is a bulky anion, whereas Zn^{2+} possesses a small ionic radius and a highly localized charge distribution, allowing OTF^{-} to approach Zn^{2+} with relatively low steric hindrance. In contrast, OTA^{4+} has a substantially larger molecular framework, and steric repulsion limits its ability to coordinate with OTF^{-} despite its high formal charge. Our MD simulations further reveal that HVOC interacts with surrounding water molecules (Fig. R22b), reducing the number of water molecules available for Zn^{2+} solvation. This decrease in Zn^{2+}–H_2O interactions increases the competitiveness of OTF^{-} to enter the Zn^{2+} primary solvation shell.

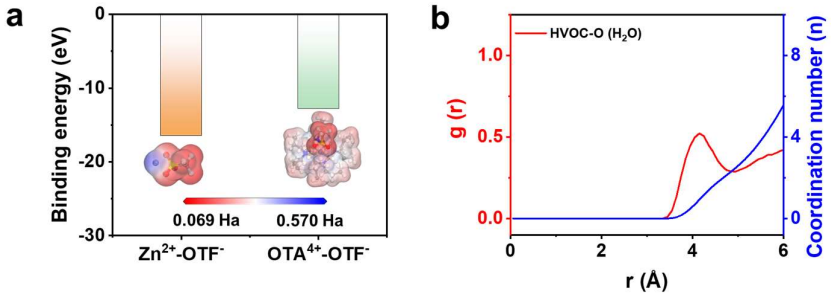

Fig. R22 a Calculated binding energies of Zn^{2+}–OTF^{-} and HVOC–OTF^{-}. **b** RDF results for HVOC–O (H_2O) obtained from MD simulations in HVOC electrolyte.

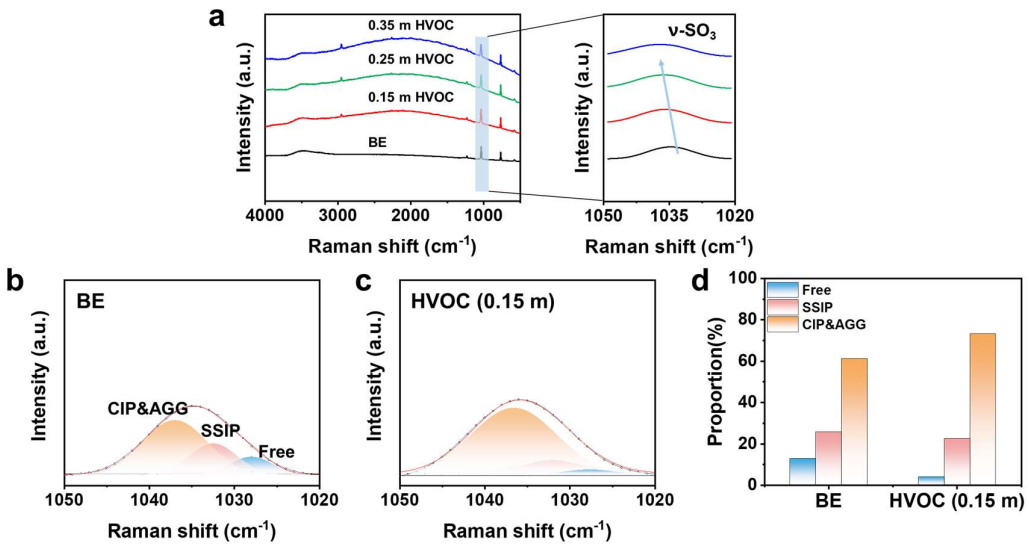

Fig. R23 a Raman spectra of H_2O, BE, and electrolytes with different concentrations of HVOC. The fitted Raman spectra of **b** BE and c HVOC (0.15 m). d The calculated free anion, SSIP and CIP&AGG area ratios.

Raman spectroscopy provides additional supporting evidence. In the 1020–1050 cm^{-1} region associated with the *v*-SO_3 stretching of OTF^-, peak deconvolution resolves free OTF^-, solvent-separated ion pairs (SSIP, ~1028 cm^{-1}), contact ion pairs (CIP, ~1032 cm^{-1}), and aggregates (AGG, ~1037 cm^{-1}). Increasing the HVOC concentration leads to a clear shift of the *v*-SO_3 band toward higher wavenumbers (Fig. R23a) and a marked increase in the fractions of CIP and AGG species (Figs. R23b-d), indicating more Zn^{2+}–OTF^- coordination. Taken together, the DFT results, MD simulations, and Raman analysis consistently indicate that HVOC enhances Zn^{2+}–OTF^- coordination by reorganizing the solvation structure that promotes OTF^- participation in the Zn^{2+} coordination environment.

We have included the corresponding data in Supplementary Information (Supplementary Figs. 21 and 23) and incorporated the relevant discussion in the revised manuscript (Page 11).

b. Authors repeatedly mention that water activity is suppressed by HVOC. How does it exactly work? Please explain in detail. In addition, in-situ Raman at bond regions of

water should be analyzed to show how water structure changes at the interface during cycling

Response. We thank the reviewer for this important question and suggestion. The suppression of water activity by HVOC can be understood from both the bulk electrolyte and the electrode interface.

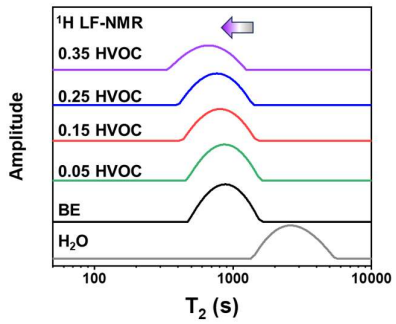

Fig. R24 ^{1}H LF-NMR spectra of H_2O and different electrolytes.

In the bulk phase, we used low-field ^{1}H nuclear magnetic resonance (LF–NMR) to monitor the T_2 relaxation time of water protons as an indicator of water activity. As the HVOC concentration increases, the T_2 value decreases, indicating that the interaction between HVOC and water molecules reduces the mobility of water and corresponds to a lower water activity.

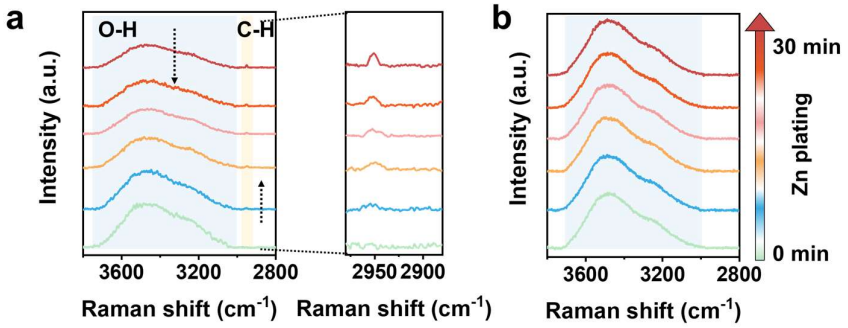

Fig. R25 In-situ Raman spectra in the range of 2800-3800 cm^{-1} of the Zn||Zn symmetrical cells with **a** HVOC and **b** BE during Zn plating.

At the interface, in-situ Raman spectroscopy further confirms the decrease in water activity and the corresponding structural changes of interfacial water. The broad band centered at 3000–3700 cm^{-1} corresponds to the O–H stretching vibration of interfacial water. A characteristic peak of HVOC appears near 2952 cm^{-1}. During Zn plating, the

2952 cm^{-1} peak gradually increase, while the O–H band decreases (Fig. R25a). This trend indicates field-induced adsorption of HVOC onto the Zn surface, which reduces the number of water molecules in close to the electrode and consequently suppresses possible water decomposition. In contrast, the BE electrolyte maintains a strong O–H stretching signal, suggesting a persistently water-rich interface (Fig. R25b).

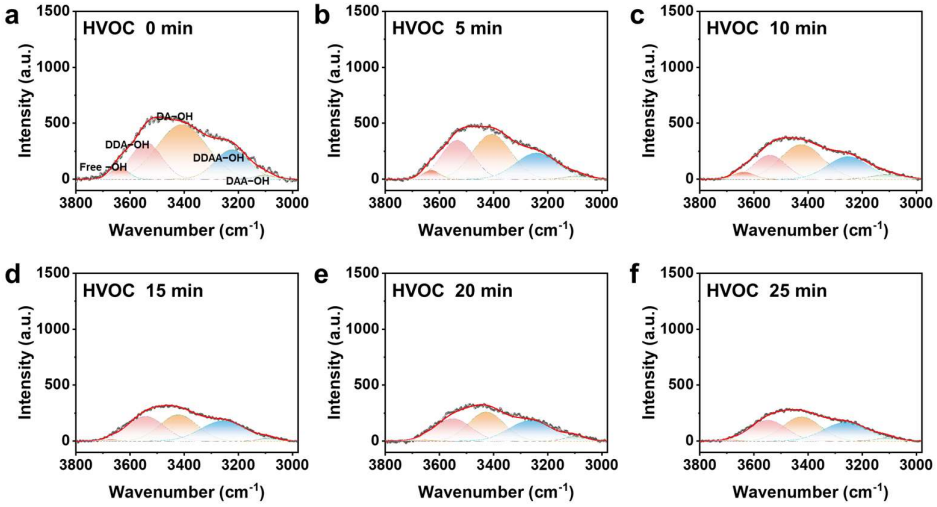

Fig. R26 The fitted Raman spectra of the Zn||Zn symmetrical cells with HVOC during Zn plating.

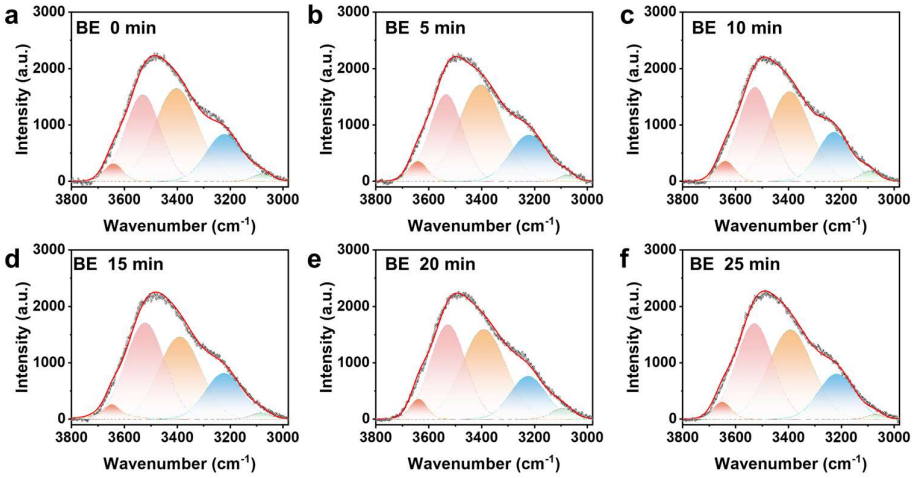

Fig. R27 The fitted Raman spectra of the Zn||Zn symmetrical cells with BE during Zn plating.

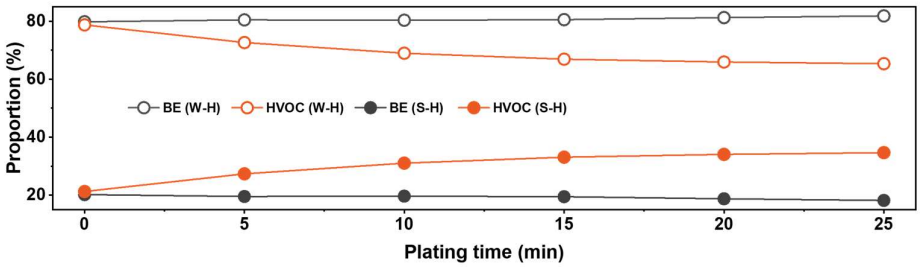

Fig. R28 The calculated HBs area ratios.

To further elucidate the interfacial water structure, we performed peak deconvolution of the 3000–3800 cm^{-1} region. According to the established proton donor (D)–acceptor (A) mechanism, the O–H stretching band consists of five components: free O–H, DDA–OH, DA–OH, DDAA–OH, and DAA–OH. Among these, free O–H, DDA–OH, and DA–OH represent weak hydrogen bonds (W–H), while DDAA–OH and DAA–OH correspond to strongly hydrogen-bonded (S–H) water (*Nat. Commun. 16:6134 (2025); J. Am. Chem. Soc. 147, 19, 16350-16361 (2025); Adv. Energy Mater. 15, e03616 (2025)*). In the HVOC electrolyte, the fraction of W–H decreases during plating (Figs. R26 and R28). This evolution indicates that HVOC adsorption suppresses the presence of activate water molecules that are capable of coordinating Zn^{2+} or participating in hydrogen evolution (*Nat. Commun. 16:6134 (2025); J. Am. Chem. Soc. 147, 19, 16350-16361 (2025)*). By lowering interfacial water activity, HVOC helps to stabilize Zn deposition and suppress parasitic reactions. In contrast, the BE system retains a high proportion of W–H water, consistent with abundant Zn-coordinated water and the higher susceptibility to side reactions (Figs. R27 and 28). These Raman results provide direct spectroscopic evidence that HVOC restructures the interfacial water network and reduces the population of reactive water species during cycling, which supports the proposed interfacial stabilization mechanism. We have included the corresponding data in Supplementary Information (Supplementary Figs. 39-42) and incorporated the relevant discussion in the revised manuscript (Pages 17-18).

c. The schematical illustration of solvation structure in both electrolytes should be provided.

Response: We thank the reviewer for this constructive suggestion. As shown in Fig. 2i of our manuscript, Zn^{2+} in BE is coordinated on average by 5.0 water molecules and 1.0 OTF^-. In the HVOC electrolyte, the coordinated average water decreases to 4.6 while OTF^- increases to 1.4, reflecting a shift toward an anion-richer solvation structure. Beyond average coordination statistics, we further analyzed the specific solvation structure surrounding Zn^{2+}. In BE, the Zn^{2+} solvation structure is dominated by $[Zn(H_2O)_6]$ (20.75%), $[Zn(H_2O)_5(OTF)_1]$ (47.17%), and $[Zn(H_2O)_4(OTF)_2]$ (30.19%), with only 1.89% of $[Zn(H_2O)_3(OTF)_3]$ species (Figs. R29a and c). In contrast, HVOC induces a significant redistribution of these motifs, most notably increasing the fraction of $[Zn(H_2O)_3(OTF)_3]$ to 15.1%. The fraction of $[Zn(H_2O)_6]$, $[Zn(H_2O)_5(OTF)_1]$, and $[Zn(H_2O)_4(OTF)_2]$ is 15.09%, 45.28%, and 24.53% respectively (Figs. R29b and c).

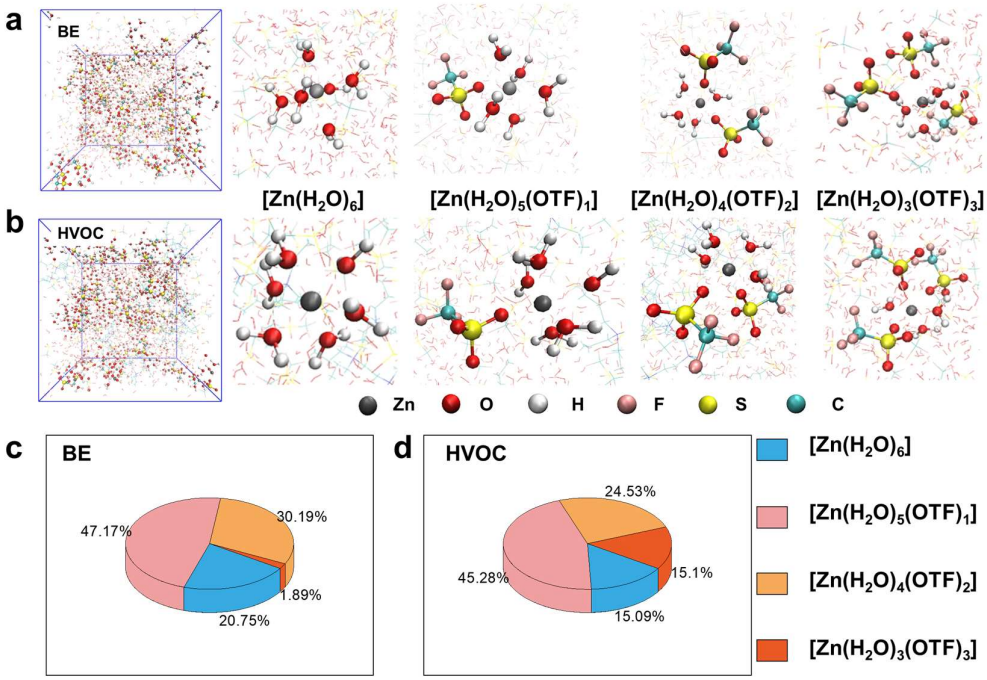

Fig. R29 The schematical illustration of solvation structure in **a** BE and **b** HVOC electrolytes. The calculated specific solvation structure ratio in **c** BE and **d** HVOC electrolytes.

We have included the corresponding schematic illustration and numerical distribution in Supplementary Information (Supplementary Fig. 20) and incorporated the relevant discussion in the revised manuscript (Page 11).

2. XPS, SEI and Zn plating kinetics

a. Why is there a N signal in BE electrolyte? There is no N-contained component in BE electrolyte if I understand it correctly.

Response: We thank the reviewer for the careful observation. As shown in our XPS results, no N 1s signal is detected for the BE electrolyte, which is consistent with the absence of N-containing species in its formulation. The very weak N-related signal observed in the TOF-SIMS mapping of the BE-cycled electrode is attributed to trace surface contaminants introduced by the conductive tape during sample testing. Importantly, the intensity of this signal is extremely low relative to that in the HVOC system and does not influence our interpretation of the interfacial chemistry. We have clarified this point in the revised manuscript (Page 13) to avoid potential misunderstanding.

b. Usually, C 1s at 284.8 eV is set as reference, not 284.4 eV. The C1s fitting spectra should be provided.

Response: We thank the reviewer for pointing this out. In our XPS analysis, the C 1s peak at 284.8 eV was indeed used as the reference for calibration, and the value 284.4 eV in the original manuscript was a typo. We have corrected this description in the revised manuscript (Page 12 and 27) and have now provided the corresponding C 1s fitting spectra (Fig. R30) in the Supplementary Information (Supplementary Fig. 28). In addition, we have carefully checked and verified all numerical values throughout the manuscript to avoid similar inaccuracies.

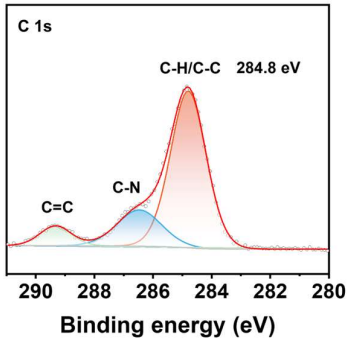

Fig. R30 The C 1s XPS fitting spectra.

c. S 2p should be fit with 2p 1/2 and 2p 3/2. It is unprofessional and unscientific to fit S2p with one peak. Much more rigorous analysis is required for XPS fitting.

Response: We thank the reviewer for this valuable comment. Following the suggestion, we have re-fitted the S 2p region using the appropriate S 2p1/2 and 2p3/2. The S 2p signals can be deconvoluted into two components. The first corresponds to SO_3 species with S 2p3/2 at 169.3 eV and S 2p1/2 at 170.5 eV. The second corresponds to ZnS_x species with S 2p3/2 at 162.2 eV and S 2p1/2 at 163.6 eV (*Angew. Chem. Int. Ed. 62, e202302583 (2023)*). The updated fitting results have been incorporated into the revised manuscript and are presented in the revised Fig. 3.

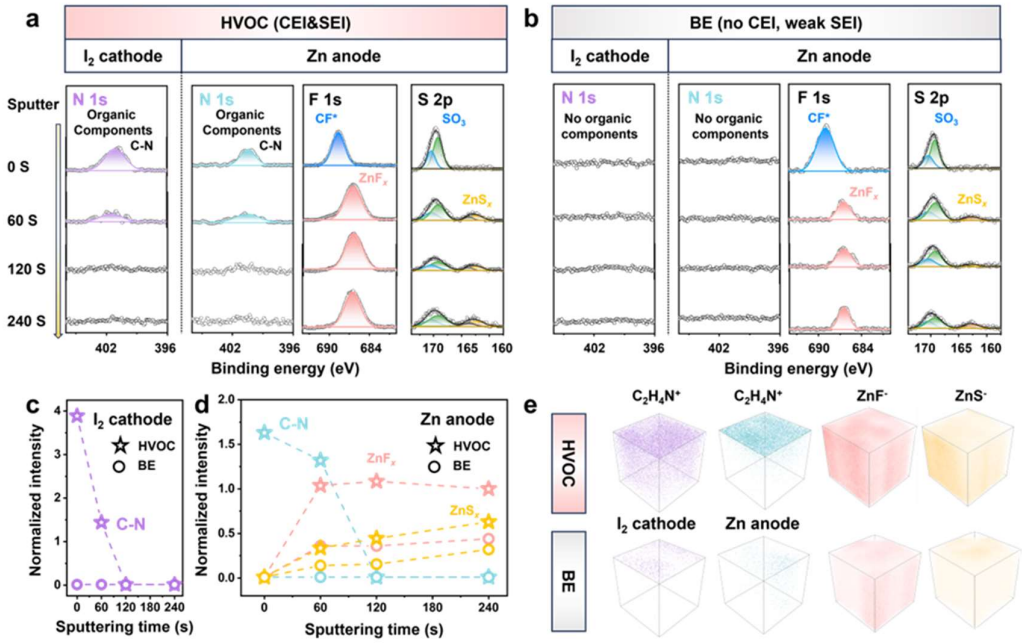

Fig. R31 The revised Fig. 3. XPS depth profiles of the I_2 cathode after cycling with **a** HVOC and **b** BE electrolytes. **c** Normalized intensity evolution of CEI-related C-N fragment at the I_2 cathode as a function of sputtering time. **d** Normalized intensity evolution of key SEI-related species at the Zn anode as a function of sputtering time. **e** 3D TOF-SIMS reconstruction images of characteristic interfacial species on both the I_2 cathode and Zn anode after cycling with different electrolytes.

d. Authors repeatedly claim that ZnS_x and ZnF_x can enhance Zn deposition kinetics. Why? How does Zn^{2+} transport in ZnS and ZnF_2? One would expect it will be slow in

such inorganic components, especially for Zn^{2+} with two charges. The electrostatic force between Zn^{2+} and these inorganic frameworks should be strong. In fact, in Fig 5g, the overpotential of BE is even lower than that of HVOC-based electrolyte.

Response: We sincerely thank the reviewer for raising this insightful question. We would like to use this chance to clarify that the role of ZnF_x and ZnS_x in enhancing Zn deposition kinetics is mechanistically distinct from the increase in nucleation overpotential observed in HVOC-based symmetrical cells. The inorganic SEI components (ZnF_x/ZnS_x) facilitate Zn^{2+} desolvation and interfacial ion transfer, whereas the increased overpotential arises from electrostatic shielding by multivalent HVOC cations, as detailed below.

Extensive prior studies have demonstrated that constructing ZnF_x or ZnS_x -rich layers, either via electrolyte formulation or interfacial engineering, can effectively lower desolvation barriers and accelerate Zn^{2+} transport across the SEI. For example, Ma *et al.* (*Adv. Mater. 33, 2007406 (2021)*) directly demonstrated that ZnF_2 exhibits exceptionally high Zn^{2+} ionic conductivity (~80.2 mS cm^{-1}) while remaining electronically insulating, thereby enabling fast Zn^{2+} transport across the interphase. Yang *et al* (*Adv. Mater. 33, 2007388 (2021)*) demonstrated the designed ZnF_2 matrix on Zn foil to redistribute Zn^{2+} flux and reduce desolvation energy, attributing the enhanced kinetics to strong Coulombic interactions between ZnF_2 and solvated Zn^{2+}, which facilitated the removal of solvation sheath in $[Zn(H_2O)_6]^{2+}$. Xie *et al.* (*Angew. Chem. Int. Ed. 62, e202216934 (2023)*) further reported that ZnF_2-rich SEI layers derived from fluoroethylene carbonate additives exhibit a stronger Zn affinity, which is in favor of regulating Zn^{2+} flux and achieving a homogeneous Zn deposition. Hao *et al* (*Adv. Mater. 32, 2003021 (2020)*) demonstrated ZnS interphases modifies the charge distribution in Zn metal and accelerates the Zn^{2+} diffusion at the ZnS@Zn interphase. Recently, Heo et al (*Joule 9, 101844 (2025)*) further emphasized the cooperative role of ZnF_2 (inner layer providing low overpotential and dendrite suppression) and ZnS (outer layer offering mechanical robustness and ionic conductivity) in stabilizing Zn deposition.

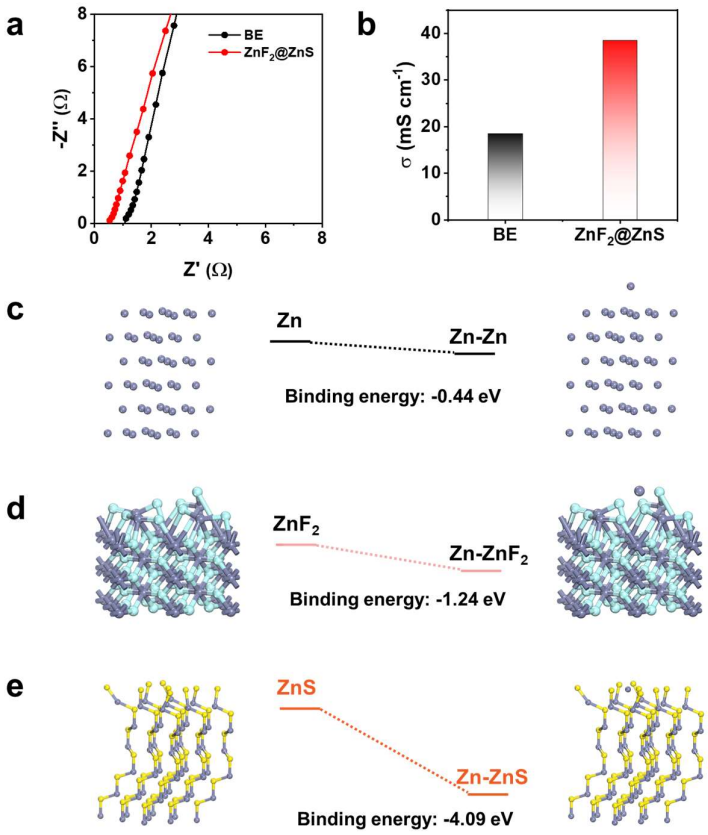

Fig. R32 a The A. C. impedance spectra and **b** the corresponding ionic conductivity (σ) of BE and ZnF_2@ZnS. The binding energy of **c** Zn metal, **d** ZnF_2 and **e** ZnS.

To support these literature findings, the ionic conductivity of the ZnF_2@ZnS-modified system was evaluated under identical measurement conditions (Figs. R32a and b). With ZnF_2@ZnS, the ionic conductivity is calculated to be 38.5 mS cm^{-1}, which is substantially higher than that of the baseline system (18.5 mS cm^{-1}). This result indicates that the ZnF_2@ZnS interphase does not hinder Zn^{2+} transport, but provides a favorable pathway for ion migration across the interface. Furthermore, we performed DFT calculations on the binding energies of Zn with Zn metal, ZnF_2, and ZnS. As shown in Figs. R32c-d, the Zn–ZnF_2 and Zn–ZnS binding energies (−1.24 eV and −4.09 eV, respectively) are significantly negative than that of Zn–Zn metal (−0.44 eV). This interaction facilitates the removal of water molecules from the Zn^{2+} solvation shell, thereby accelerating Zn^{2+} desolvation and enhancing ion transport kinetics. Regarding the Zn^{2+} transport mechanism at the ZnS and ZnF_2 interfaces, our findings, together with prior reports, indicate that Zn^{2+} ions are not transported through the bulk phases

of ZnS or ZnF_2, but rather through surface-facilitated desolvation processes (*Angew. Chem. Int. Ed. 63, e202401987 (2024); Energy Environ. Sci. 18, 1683-1695 (2025)*). We have included the corresponding data in Supplementary Information (Supplementary Fig. 29) and incorporated the relevant discussion in the revised manuscript (Page 13).

With regard to the observation that the overpotential in the HVOC-based symmetrical cell is higher than in the BE (Fig. 5g), we agree with the reviewer that this may initially appear counterintuitive. However, this phenomenon is well-documented in the context of multivalent cation–modified aqueous electrolytes. Prior studies (*Nat. Commun. 13, 3252 (2022); Angew. Chem. Int. Ed. 61, e202211589 (2022); Adv. Mater. 34, 2203104 (2022); Energy Environ. Sci. 16, 4561 (2023)*) have shown that the presence of high-valent species such as La^{3+}, Sc^{3+}, Ce^{3+}, or Zr^{4+} can induce interfacial electrostatic shielding or competitive adsorption with Zn^{2+} at the Zn surface, leading to increased nucleation overpotentials. Therefore, although HVOC introduction promotes more favorable Zn^{2+} solvation and SEI composition, the rise in overpotential originates from cation–surface interactions, not from slower Zn^{2+} transport in ZnF_x/ZnS_x. We hope this clarification addresses the reviewer's concerns. We have incorporated the relevant discussion in the revised manuscript (Page 21).

e. "This robust inorganic phase provides excellent electronic insulation and mechanical strength, effectively accommodating volume changes and relieving interfacial stress during repeated Zn plating/stripping." Why? Please provide the evidence.

Response: We thank the reviewer for this thoughtful comment. To substantiate the statement that the ZnF_2/ZnS-rich SEI provides electronic insulation, we first evaluated its intrinsic electronic properties by DFT. The calculated band gap energies are 4.8 eV for ZnF_2 and 2.28 eV for ZnS, characteristic of an insulating phase and a wide-band-gap semiconductor (Fig. R33a), respectively, and therefore far less electronically conductive than metallic Zn. Consistently, direct resistance measurements of Zn electrodes coated with ZnF_2/ZnS show resistances exceeding the instrumental detection

limit, confirming that these SEI components act as electronically blocking layers (Fig. R33b). Such electronic insulation prevents electrons from leaking into the electrolyte and allows Zn^{2+} ions to migrate through the SEI without being prematurely reduced, which favors more homogeneous Zn deposition beneath the SEI (*Energy Environ. Sci. 18, 1683-1695 (2025); Adv. Funct. Mater. DOI: 10.1002/adfm.202523560 (2025)*).

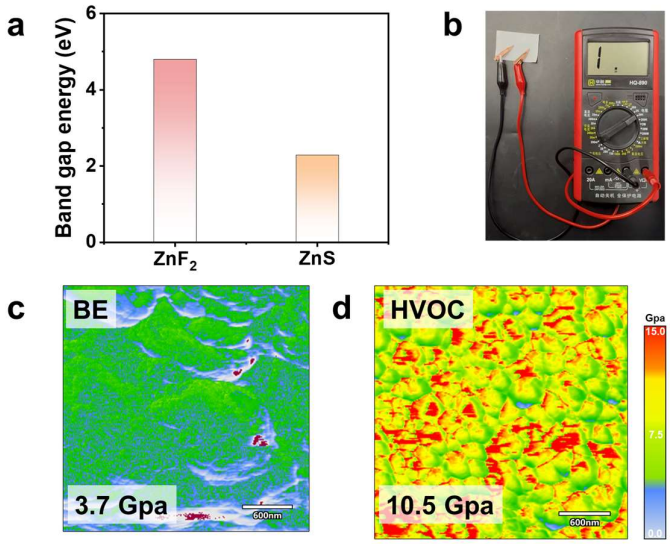

Fig. R33 a The band gap energy of the ZnF_2 and ZnS. **b** Multimeter measurement of the surface resistance of the Zn electrode coated with ZnF_2/ZnS. The average Young's modulus of the cycled Zn anode in **c** BE and **d** HVOC.

To support the claim that the SEI provides mechanical robustness and helps accommodate volume changes during cycling, we performed AFM based nanoindentation measurements on Zn anodes after cycling in different electrolytes. As shown in Figs. R33c and d, the average Young's modulus of SEI layers formed on the Zn anode cycled in the HVOC electrolyte is 10.5 GPa, significantly higher than the 3.7 GPa measured for the BE. This increase in modulus is attributed to the formation of robust ZnF_2/ZnS rich SEI. A mechanically stronger interphase can better resist local deformation, distribute plating and stripping induced stress more uniformly, and thereby help accommodate repeated volume changes during Zn cycling (*Angew. Chem. Int. Ed. 62, e202216934 (2023); Angew. Chem. Int. Ed. 63, e202401987 (2024); Environ. Sci. 18, 1683-1695 (2025)*). We have included the corresponding data in

Supplementary Information (Supplementary Fig. 30) and incorporated the relevant discussion in the revised manuscript (Page 13).

f. Authors mentioned that ZnF_x/ZnS_x SEI lowers the charge-transfer resistance, however, the R_{ct} is actually higher in HVOC electrolyte in Fig S26.

Response: We thank the reviewer for the academic suggestion. To accurately interpret the charge-transfer resistance, it is essential to consider its evolution throughout cycling rather than relying on a single comparison point. As shown in Supplementary Fig. 48 (original Fig S26), the HVOC electrolyte exhibits a lower R_{ct} than BE in the initial cycle, reflecting facilitated interfacial charge transfer kinetics at the early stage.

For the BE electrolyte, the rapid decrease in R_{ct} during subsequent cycles does not indicate improved interfacial kinetics. Instead, it is associated with nonuniform Zn nucleation and tip-favored Zn accumulation. The same trend of charge transfer resistance for the bare electrolyte is also confirmed by the literature of *Energy Environ. Sci. 16, 1662-1675 (2023) (Fig. S19)*, and they attribute this to the nonuniform Zn plating behavior in the bare electrolyte. During the plating and striping process of the Zn||Zn battery with BE, Zn^{2+} tends to accumulate at the tips due to uncontrolled Zn nucleation and deposition behavior, which lowers R_{ct} in the early cycles. For HVOC, the interfacial resistance initially increased due to the formation of an in situ adsorbed cationic layer, then gradually decreased and stabilized as ZnF_x and ZnS_x-rich SEI formed, facilitating ion transport and lowering R_{ct}. These points have been incorporated and highlighted in the revised manuscript on page 20.

3. For most of physical characterization and simulations, the exact electrolyte formula is missing. In addition, is $Zn(OTf)_2$ concentration an important factor? 3m is a relatively high concentration. Does this strategy apply to more cost-friendly $ZnSO_4$?

Response: We thank the reviewer for raising this important point. Accordingly, we have added the exact compositions of all electrolytes used in physical characterizations and simulations to the revised manuscript. Specifically, the electrolytes for in situ UV–vis

and Raman measurements were 3 m $Zn(OTF)_2$ (BE), 0.15 m MVOC, and 0.15 m HVOC. For NMR and LF–NMR measurements, we used water, BE, and HVOC with concentrations of 0.05 m, 0.15 m, 0.25 m, and 0.35 m. The 2D LF ^1H T_1–T_2 mapping was performed using water and 0.15 m HVOC. Raman spectra were collected for water, BE, and HVOC at 0.15 m, 0.25 m, and 0.35 m. The electrolyte compositions used in the MD simulations have been summarized in Table R2 and added to the Supplementary Information (Supplementary Table 3).

Table R2 Simulated electrolyte compositions.

Electrolyte	Number			
	Zn^{2+}	OTF^-	DAA^+	OTA^{4+}
BE	144	288	-	-
MVOC	144	302	14	-
HVOC	144	344	-	14

Regarding the effect of $Zn(OTF)_2$ concentration, we evaluated the electrochemical behavior by fixing the HVOC content at 0.15 m and preparing electrolytes containing 1 m, 2 m, and 3 m $Zn(OTF)_2$. As shown in Fig. R34a, Zn||Cu and Zn||Zn cells demonstrate stable Zn reversibility in the 2 m and 3 m electrolytes at 1 mA cm^{-2}, 5 mAh cm^{-2}, with the 3 m formulation exhibiting slightly improved performance. In contrast, the 1 m electrolyte shows pronounced initial polarization and cannot sustain stable operation. Contact-angle measurements on the I_2 electrode further reveal that increasing the $Zn(OTF)_2$ concentration enhances surface wettability. Full-cell performance also shows that Zn–I_2 batteries using 2 m and 3 m $Zn(OTF)_2$ exhibit comparable cycling stability, with the 3 m electrolyte providing a marginal advantage. These observations suggest that $Zn(OTF)_2$ concentrations in the range of 2-3 m are suitable for achieving balanced Zn reversibility and cathode–electrolyte interfacial compatibility.

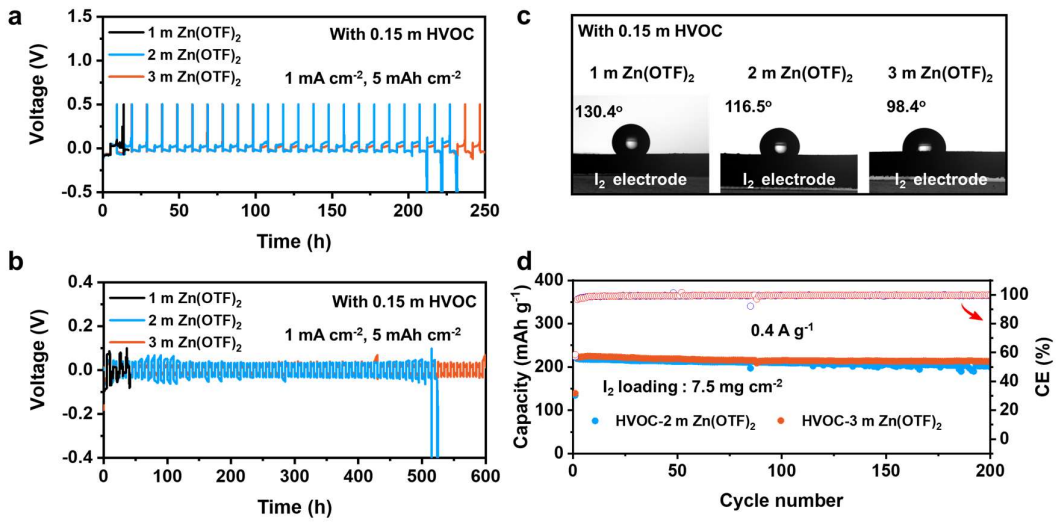

Fig. R34 a Long-term cycling stability of Zn||Cu cells at 1 mA cm^{-2}, 5 mAh cm^{-2} with 0.15 m HVOC at different $Zn(OTF)_2$ concentration. **b** Long-term cycling stability of Zn||Cu cells at 1 mA cm^{-2}, 5 mAh cm^{-2} with 0.15 m HVOC at different $Zn(OTF)_2$ concentration. **c** Contact angle of different electrolytes on I_2 electrode surface. **d** Cycling stability of Zn–I_2 battery with HVOC at different $Zn(OTF)_2$ concentrations.

To assess the broader applicability of the high-valent organic cation strategy, we further evaluated $ZnSO_4$-based electrolytes containing MVOC or HVOC (Fig. R35). At a current density of 1 mA cm^{-2} with an area capacity of 5 mAh cm^{-2}, Zn||Zn and Zn||Cu cells with MVOC- or HVOC-containing $ZnSO_4$-based electrolytes exhibit markedly improved Zn reversibility compared with the bare $ZnSO_4$. In full Zn–I_2 batteries, the HVOC-containing $ZnSO_4$-based electrolyte delivers superior cycling stability and stable CE, outperforming not only the BE electrolyte but also the MVOC-containing system. These results demonstrate that the high-valent organic cation strategy is not limited to $Zn(OTF)_2$ and can also be applied in more cost-effective $ZnSO_4$-based electrolytes.

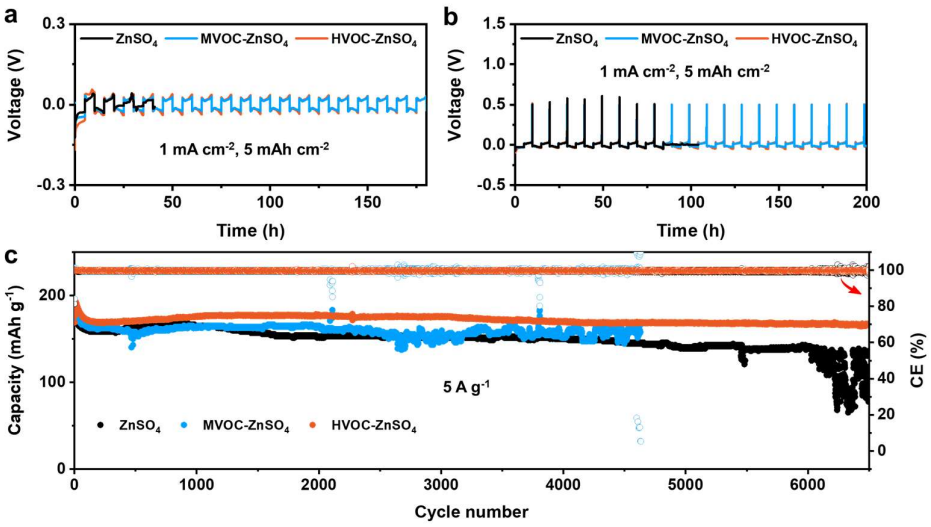

Fig. R35 a Long-term cycling stability of Zn||Cu cells at 1 mA cm^{-2}, 5 mAh cm^{-2} with HVOC in $ZnSO_4$-based electrolytes. **b** Long-term cycling stability of Zn||Cu cells at 1 mA cm^{-2}, 5 mAh cm^{-2} with HVOC in $ZnSO_4$-based electrolytes. **c** Cycling stability of Zn–I_2 battery with HVOC in $ZnSO_4$-based electrolytes.

The corresponding data and discussion have been added to the revised Supplementary Information (Supplementary Figs. 51 and 64) and revised manuscript (Pages 20 and 24).

4. For CA analysis, please explain in detail or clearly label 2D vs. 3D contribution. Right now, it is confusing.

Response: We thank the reviewer for this professional suggestion. Following the comment, we have revised the chronoamperometry (CA) analysis to clearly distinguish the two-dimensional (2D) diffusion-controlled nucleation stage from the subsequent three-dimensional (3D) growth stage, following the methodology reported in the literature *Angew. Chem. Int. Ed. 64, e202504965 (2025)* and *Energy Environ. Sci. 16, 6026 (2023)*. In the fitting process, we mainly adopted the following equations:

$$I = I_{dl} + I_{dep}$$

$$I_{dl} = I_0 \cdot e^{-\frac{t}{\tau}}$$

$$I_{dep} = I_{2D} + I_{3D}$$

$$I_{2DI}(t) = a_{2DI} \cdot t \cdot \exp(-b_{2DI} \cdot t^2)$$

$$I_{2DP}(t) = a_{2DP} \cdot t^2 \cdot \exp(-b_{2DP} \cdot t^3)$$

$$I_{3DI}(t) = c_{3DI} \cdot [1 - \exp(-d_{3DI} \cdot t^2)$$

$$I_{3DP}(t) = c_{3DP} \cdot [1 - \exp(-d_{3D} \cdot t^3)$$

In this analysis, I_{2DI}, I_{2DP}, I_{3DI}, I_{3DP} and I_{dl} correspond to the current contributions from two dimensional instantaneous nucleation, two-dimensional progressive nucleation, three dimensional instantaneous nucleation, three-dimensional progressive nucleation and double layer, respectively. The parameters a, b, c, d, and τ are related describe system-specific physicochemical characteristics.

The fitted results reveal distinct differences among BE, MVOC, and HVOC. In BE, Zn nucleation undergoes a prolonged 2D diffusion-controlled regime (97 s) (Fig. R36a), indicating a low nucleation density and the formation of relatively large Zn nuclei, which is unfavorable for uniform growth and promotes the formation of dendritic morphologies (*Angew. Chem. Int. Ed. 64, e202504965 (2025)*). In the MVOC electrolyte, the duration of the 2D region is shortened (67 s) (Fig. R36b), suggesting a moderate improvement in nucleation behavior. In contrast, the HVOC electrolyte exhibits an obvious shorter 2D diffusion regime (21 s) and transitions rapidly into the 3D growth region (Fig. R36c). This accelerated transition corresponds to a higher nucleation density and enables more uniform Zn deposition, thereby suppressing dendrite formation. The revised CA plots with clearly labeled 2D and 3D regions, together with the corresponding fitting equations, have been included in the updated Supplementary Information.

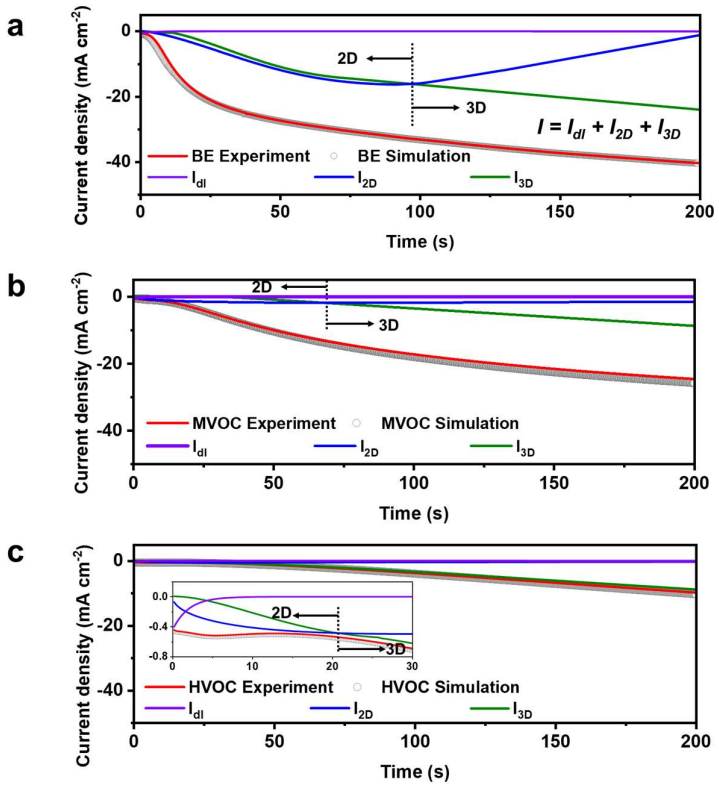

Fig. R36 Chronoamperometry curves and fitted I_{dl}, I_{2D}, and I_{3D} contribution for Zn||Zn cells in **a** BE, **b** MVOC and **c** HVOC.

We have included the corresponding data in Supplementary Information (Supplementary Fig. 46) and incorporated the relevant discussion in the revised manuscript (Pages 19 and 20).

5. Fig 4i, why does a 0.997 r^2 indicates the highly reversible redox process? The behind equations and logic should be presented in more detail.

Response: We appreciate the reviewer's professional comment. In our analysis, we used the Randles–Sevcik relationship for electrochemically reversible redox processes (*J. Chem. Educ. 95, 197-206 (2018)*), which describes the dependence of the peak current i_p on the scan rate:

$$i_p = 0.446\, nFAC^0 \left(\frac{nFD_0}{RT}\right)^{1/2} \nu^{1/2}$$

where n is the number of transferred electrons, A is the electrode surface area, C^0 is the bulk concentration of the redox species, D_0 is the diffusion coefficient, ν is the

scan rate, and F , R, and T is the Faraday constant, universal gas constant and temperature, respectively. Under fixed experimental conditions, all parameters except ν are constant, so a reversible redox process is expected to show a linear dependence of i_p on $\nu^{1/2}$.

As shown in Fig. 4i, the reduction peak current density of R1 exhibits a good linear correlation with $\nu^{1/2}$ in all three electrolytes, which is consistent with electrochemically reversible iodine redox behaviour. The corresponding correlation coefficients are 0.997, 0.994, and 0.990 for HVOC, MVOC, and BE, respectively. The highest R^2 value obtained for the HVOC electrolyte indicates that the R1 process in HVOC most closely follows the Randles–Sevcik prediction and therefore exhibits more ideal reversible kinetics than in the other two systems (*J. Am. Chem. Soc. 146, 31, 21377-21388 (2024)*). In the revised manuscript, we have added the Randles–Sevcik equation (Page 17) and further clarified the physical meaning behind the R^2 analysis to improve clarity (Supplementary Note 5).

Reviewer #3:

This work presents an innovative electrolyte design strategy using high-valence organic cations to regulate both the iodine cathode and Zn anode interfaces. The approach effectively mitigates polyiodide shuttle and Zn corrosion, delivering high capacity and stable cycling under various practical conditions. The underlying mechanisms have also been elucidated through detailed characterizations. With sufficient novelty in electrolyte design and clear performance improvement, this work should be of interest to researchers in the field. Therefore, I recommend its publication in Nature Communications after addressing the following concerns.

Response: We sincerely thank the respected Reviewer's time and effort for evaluating our manuscript, as well as the positive and constructive comments. According to the Reviewer's suggestions, we have carefully revised our manuscript. The following is the point-by-point response to all the questions. We hope you will find the revised manuscript has satisfactorily addressed your concerns.

1. The discussion on EDL structures in different electrolyte systems is incomplete without considering the MVOC system. Simulation data for MVOC under the same electric field conditions as HVOC are necessary to convincingly highlight the advantages of HVOC.

Response: We thank the reviewers for these important comments. To strengthen the analysis of interfacial behavior, we expanded our simulations from a single-electrode configuration to a full-cell molecular dynamics (MD) model in which both electrodes were polarized simultaneously in BE, MVOC and HVOC systems. This framework enables quantitative assessment of ion and solvent distributions under the coupled electric fields characteristic of discharge and charge, thereby capturing the electrode–electrolyte interactions more rigorously.

As shown in Fig. R37a, the BE electrolyte forms a water-rich interfacial layer at the iodine cathode during discharge. These interfacial water molecules are highly reactive and facilitate the dissolution of polyiodide species and I_2, giving rise to pronounced shuttle effects and rapid capacity decay. In contrast, MVOC and HVOC exhibit distinct interfacial structures under the same conditions. Driven by the applied electric field, MVOC or HVOC molecules migrate toward the cathode, forming cation-enriched and water-deficient interfacial layers (Figs. R37b and R37c). The corresponding ion distribution profiles (Figs. R38a and R38b) corroborate this interfacial enrichment, while the water density profiles (Fig. R38c) further show that HVOC achieves the most pronounced suppression of interfacial water.

For the charging state at the Zn anode, the reviewers' concerns were directly examined. In BE, the absence of cationic species leads to persistently water-rich interfaces at both the cathode and anode (Fig. R37a). In the MVOC system, the lower charge density of MVOC results in substantial field-driven migration toward the I_2 electrode, leaving negligible interfacial coverage at the Zn anode (Figs. R37b and R38a). In contrast, HVOC maintains a measurable interfacial presence at the Zn anode, which increases the separation between water molecules and the electrode compared with BE and MVOC (Figs. R37c, R38b and d).

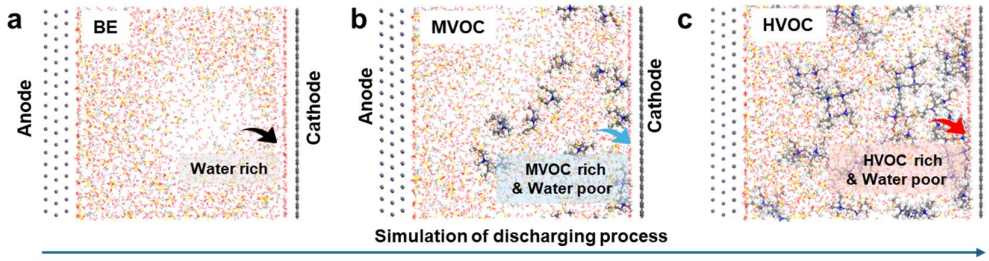

Fig. R37 MD simulated EDL configuration near the I_2 cathode and Zn anode with **a** BE, **b** MVOC and **c** HVOC during discharging.

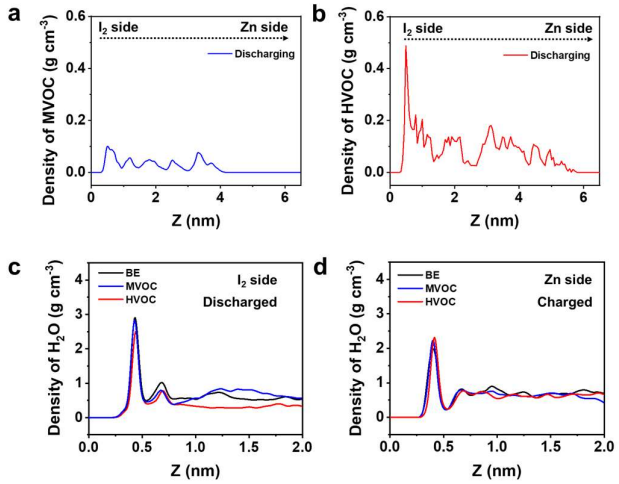

Fig. R38 **a** Corresponding cumulated density distributions of MVOC in MVOC electrolyte. **b** Corresponding cumulated density distributions of HVOC in HVOC electrolyte. **c** Corresponding cumulated density distributions of water molecules near discharged I_2 cathode in different electrolytes. **d** Corresponding cumulated density distributions of water molecules near discharged Zn anode in different electrolytes.

To further analyze the evolution of the interfaces across different electrochemical states, we reversed the field polarity to simulate the transition from discharge to charge (Fig. R39). In BE, the interfacial environment remains water-rich at both electrodes (Figs. R39a and d). For MVOC and HVOC (Figs. R39b-f), the simulations reveal that HVOC remains partially accumulated at the iodine cathode during charging, thereby suppressing undesired redox side reactions. At the same time, both MVOC and HVOC migrate toward the Zn anode and form cation-enriched layers that increase the separation between water molecules and the electrode surface.

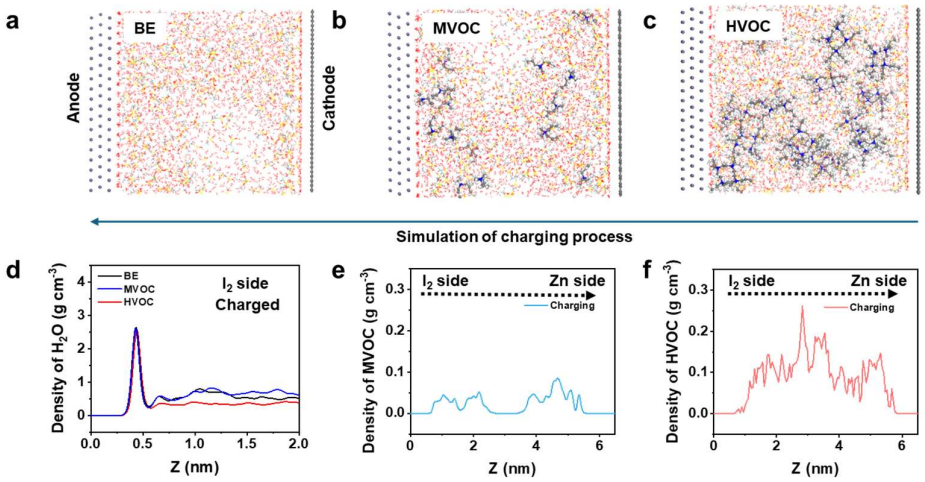

Fig. R39 MD simulated EDL configuration near the I_2 cathode and Zn anode with **a** BE, **b** MVOC and **c** HVOC during charging. **d** Corresponding cumulated density distributions of water molecules near charged I_2 cathode in different electrolytes. **e** Corresponding cumulated density distributions of MVOC in MVOC electrolyte. **f** Corresponding cumulated density distributions of HVOC in HVOC electrolyte.

The corresponding data and discussion have been added to the revised Supplementary Information (Supplementary Figs. 13-15) and revised manuscript (Pages 8-10 and Figs. 2a-d).

2. Despite the HVOC-based electrolyte exhibiting lower desolvation energy compared to BE, it presents a higher overpotential in symmetrical cell tests. The authors should provide a detailed discussion to explain this phenomenon.

Response: We appreciate the reviewer's insightful comment. Although the HVOC electrolyte shows a lower Zn^{2+} desolvation energy, the symmetrical cell indeed exhibits a higher nucleation overpotential compared with BE. This behavior is consistent with previous reports on multivalent cation modified aqueous electrolytes. Studies involving La^{3+}, Sc^{3+}, Ce^{3+}, and Zr^{4+} (*Nat. Commun. 13, 3252 (2022); Angew. Chem. Int. Ed. 61, e202211589 (2022); Adv. Mater. 34, 2203104 (2022); Energy Environ. Sci. 16, 4561 (2023)*) have demonstrated that high-valent species can competitively adsorb on Zn surfaces or introduce strong electrostatic interactions, which increase the nucleation barrier despite facilitating subsequent Zn^{2+} desolvation and deposition. We have

incorporated the relevant discussion in the revised manuscript (Page 21).

3. The authors claim that HVOC optimizes Zn nucleation morphology based on chronoamperometry measurements. It is recommended that additional experimental evidence, such as microscopic characterization, be provided. Such data would also help clarify how nucleation behavior influences interfacial stability and electrochemical performance.

Response: We appreciate the reviewer's helpful suggestion. To directly validate the nucleation behavior inferred from the chronoamperometry results, we performed SEM imaging on Cu substrates after Zn deposition at 0.05 mA cm^{-2} for 10 min. As shown in Figs. R40a and b, the BE electrolyte produces sparse, irregularly shaped Zn nuclei with significantly larger feature sizes, indicative of low nucleation density and heterogeneous early-stage growth. In contrast, Figs. R40c and d show that the HVOC-containing electrolyte yields much smaller, more densely distributed, and more uniformly shaped nuclei, demonstrating a substantially higher nucleation density and more homogeneous nucleation process. This microscopic evidence is fully consistent with the chronoamperometry-derived nucleation analysis and confirms that HVOC accelerates the transition from 2D nucleation to 3D growth.

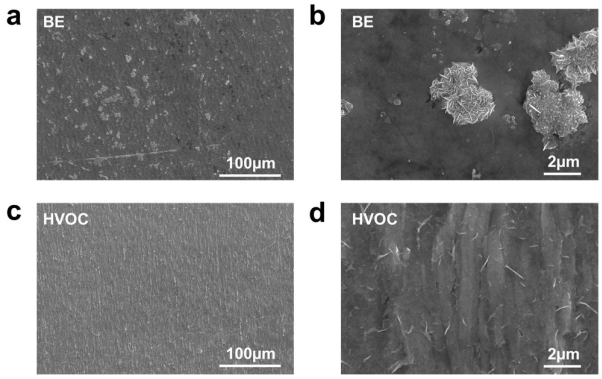

Fig. R40 The SEM images for Zn nucleation characterization in **a,b** BE and **c,d** HVOC electrolytes at a current density of 0.05 mA cm^{-2} for 10 min.

We have included the corresponding data in Supplementary Information (Supplementary Fig. 47) and incorporated the relevant discussion in the revised manuscript (Page 20).

4. Considering the effect of concentration polarization, the authors should include a comparison of Zn^{2+} diffusion coefficients in different electrolyte systems. This data would provide valuable insight into the mechanisms underlying the long-term cycling stability of Zn–I_2 batteries.

Response: We appreciate the reviewer's constructive suggestion. To further evaluate ion transport behavior, we measured Zn^{2+} diffusion coefficients using galvanostatic intermittent titration (GITT). As shown in Fig. R41 the HVOC electrolyte exhibits diffusion coefficients in the range of 2.2×10^{-8} to 3.3×10^{-7} cm^2 s^{-1}, which are higher than those of MVOC (5.7×10^{-8} to 1.5×10^{-7} cm^2 s^{-1}) and markedly exceed those of BE (7.8×10^{-9} to 1.4×10^{-7} cm^2 s^{-1}). These results demonstrate that HVOC provides significantly improved Zn^{2+} transport kinetics, helping to alleviate concentration polarization and contributing to its superior long-term cycling stability.

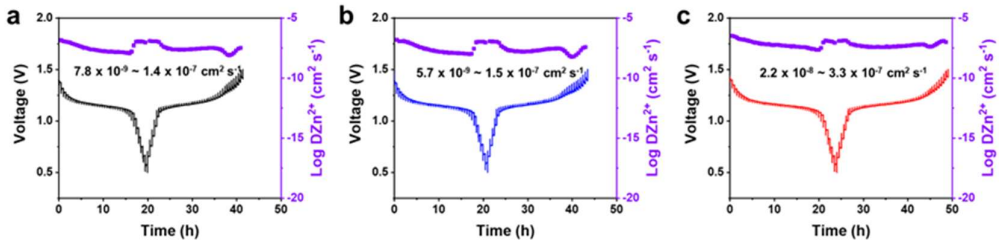

Fig. R41 GITT curves and the corresponding Zn^{2+} diffusion coefficients of Zn–I_2 batteries with **a** BE, **b** MVOC and **c** HVOC.

We have included the corresponding data in Supplementary Information (Supplementary Fig. 38) and incorporated the relevant discussion in the revised manuscript (Page 17).

5. At 5 A g^{-1}, the HVOC-based Zn–I_2 battery indeed shows longer cycling stability than BE and MVOC, which is encouraging. However, can this superiority be maintained at lower current densities (for example 0.2 A g^{-1}). where side reactions are typically more pronounced.

Response: We appreciate the reviewer's important comment. As shown in Fig. RS42, at a low current density of 0.2 A g^{-1}, batteries using BE and MVOC-based electrolytes exhibited rapid capacity fading with capacity retention of 51.3% and 61.6% after 400

cycles, respectively. In stark contrast, batteries using HVOC-based electrolyte maintained a highly stable cycling performance with 85.0% capacity retention over 400 cycles, confirming its effective suppression of undesired side reactions even at a lower current density of 0.2 A g^{-1}.

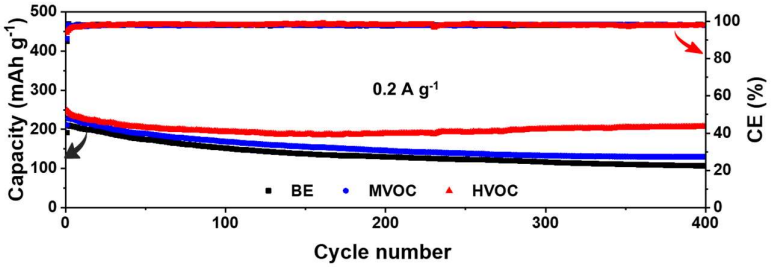

Fig. R42 Cycling stability of Zn–I_2 battery with different electrolytes at 0.2 A g^{-1}.

We have included the corresponding data in Supplementary Information (Supplementary Fig. 56) and incorporated the relevant discussion in the revised manuscript (Pages 21-22).

6. The manuscript shows that HVOC improves Zn nucleation and deposition. However, its effect on Zn corrosion resistance is not examined. Given the corrosion issues in Zn–I_2 batteries, could the authors provide relevant characterization and compare the HVOC-based electrolyte with BE and MVOC systems? Such analysis is important for assessing Zn anode stability and battery reversibility.

Response: We appreciate the reviewer's valuable suggestion. To assess the corrosion behavior of Zn, we conducted Tafel measurements for BE, MVOC, and HVOC electrolytes. As shown in Fig. R43, the HVOC electrolyte exhibits a larger corrosion potential and lower corrosion current than BE and MVOC, indicating a reduced corrosion tendency and slower corrosion rate. These results confirm that HVOC not only regulates Zn nucleation and deposition but also mitigates Zn corrosion, thereby contributing to the improved reversibility of the Zn anode.

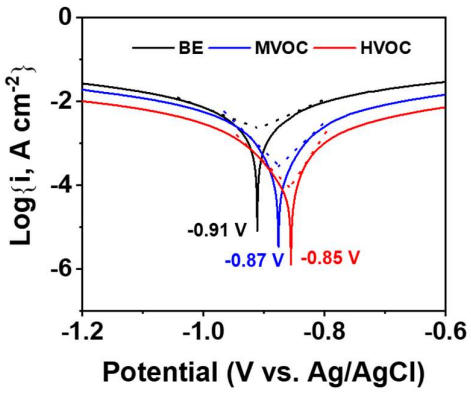

Fig. R43 Tafel curves for different electrolytes.

We have included the corresponding data in Supplementary Information (Supplementary Fig. 45) and incorporated the relevant discussion in the revised manuscript (Page 19).

7. To improve the reproducibility of pouch cell performance, could the authors provide comprehensive and detailed information regarding the pouch cell assembly? It is recommended to include these details in Supplementary Information.

Response: We appreciate the reviewer's detailed suggestions. To enhance the reproducibility and transparency of our pouch cell evaluation, we have now provided a comprehensive description of the assembly protocol. Key parameters, including electrode dimensions, active material loading, electrolyte amount, separator type, and current collector, have been summarized in a dedicated table (Table R3). This information has been added to the revised Supplementary Information as Supplementary Table 1.

Table R3: The parameters of the 0.14 Ah pouch cell.

Positive electrode (I_2)	Length (mm)	55
	Width (mm)	55
	Piece (number)	2

	Areal capacity (mA h cm^{-2})	2.3
	Loading mass (mg cm^{-2})	10.1
Electrolyte (HVOC)	Volume (mL)	~ 2
	Weight (g)	~ 2.3
Separator (GF A)	Length (mm)	60
	Width (mm)	60
	Thickness (mm)	0.25
	Weight (g)	0.25
Negative electrode (Zn Metal)	Length (mm)	55
	Width (mm)	55
	Thickness (μm)	22
	Weight (g)	0.61
	Piece (number)	3
Current collector (Ti mesh)	Length (mm)	55
	Width (mm)	55
	Mesh (number)	100
	Weight (g)	0.80

Below please check for our **point-by-point responses to the reviewers' comments**, which is also incorporated into our revised manuscript.

Enumerated responses to comments from the reviewers.

Blue type: Reviewers' comments; **Black italic**: Our responses; Red type: Notable changes.

The corresponding update has been highlighted in Yellow in the revised manuscript.

Response to Reviewers

Reviewer #1:

This study proposes the use of a high-valent organic cation (HVOC) to construct dual interfaces to improve the stability of Zn-I_2 batteries, demonstrating promising performance. Although the authors have provided point-by-point responses to the concerns and addressed some related questions, in terms of innovation, this work still does not possess the potential for publication in Nature Communications. As a polyiodide adsorption system, it fails to raise a novel concept, and extensive literature already exists on cationic additives capable of adsorbing polyiodide ions (Adv. Energy Mater. 2024, 14, 2402306; Nat Commun 16, 4586 (2025); Energy Environ. Sci., 2025, 18, 4800-4810) and improving Zn anode deposition behavior (Adv. Mater. 2024, 36, 2408287. Adv. Energy Mater. 2022, 12, 2102780; J. Am. Chem. Soc. 2025, 147, 10, 8523–8533; J. Am. Chem. Soc., 2024, 146, 21377–21388). At its core, this research merely introduces a similar molecule, which is not irreplaceable. Furthermore, the revised manuscript has introduced new issues, and some existing problems remain inadequately substantiated:

Response: We sincerely thank the reviewer for the careful evaluation of our manuscript and for pointing out these representative studies on cationic additives for regulating polyiodide species and Zn anode deposition behavior. We greatly appreciate this comment, as it provides an opportunity to further clarify and highlight the novelty of our work. We respectfully clarify that the central concept of this study is not simply the introduction of another polyiodide adsorption molecule. Rather, the key objective of

this work is to establish a **cation-valence-governed electrolyte design principle** for regulating electrode–electrolyte interfaces in aqueous Zn–I_2 batteries. Previous studies indeed demonstrated that **mono-valent organic cations (MVOCs)** can interact with polyiodide intermediates or influence Zn deposition behavior. However, these strategies primarily rely on **molecular adsorption or electrostatic shielding effects associated with mono-valent cations**, which inherently limit the strength and persistence of interfacial electrostatic interactions.

Moving beyond monovalent organic cations, this work introduces **high-valent organic cations (HVOCs)** as a new design strategy, where **cation valence is used as a key parameter to regulate electrostatic interactions at battery interfaces**. According to Coulomb's law ($F = q_1q_2/4\pi\varepsilon d^2$), increasing ionic charge significantly strengthens electrostatic interactions. Based on this principle, the tetravalent cation introduced in this work forms a highly charged electrostatic center, enabling much stronger and more persistent interfacial interactions than those achievable with conventional mono-valent cations.

Regarding the studies cited by the reviewer on iodine cathode regulation (*Adv. Energy Mater. 2024, 14, 2402306; Nat. Commun. 2025, 16, 4586; Energy Environ. Sci. 2025, 18, 4800–4810*), these works primarily rely on **mono-valent cation adsorption to confine polyiodide intermediates**. In comparison, the HVOC electrolyte developed in this work exhibits **superior cycling stability and capacity retention** relative to these reported monovalent cation systems (Table R1), highlighting the advantage of stronger electrostatic confinement enabled by high-valent cations. For the Zn anode, the studies cited by the reviewer (*Adv. Mater. 2024, 36, 2408287; Adv. Energy Mater. 2022, 12, 2102780; J. Am. Chem. Soc. 2025, 147, 8523–8533; J. Am. Chem. Soc. 2024, 146, 21377–21388*) mainly employ mono-valent cations to regulate Zn deposition through electrostatic shielding or crystallographic orientation manipulation. These strategies can influence Zn deposition behavior but typically do not establish a **persistent cation-derived interfacial layer** on the Zn surface.

Table R1. A comparison of Zn–I_2 battery performance.

Modified strategies		Z	I_2 loading (mg cm^{-2})	Cycling performance	Temperature (°C)	Ref.
HVOC-based	$OTF(OTF)_4$	**+4**	**2**	**99.9%@130 cycles**	**-40**	***This work***
			22	**97.2%@250 cycles**	**25**	
			17.1	**86.1@100 cycles**	**60**	
MVOC-based	TMAF	+1	1.5	~95.5%@250 cycles	30	[1]
	TMAI		15	91.3@100 cycles	25	[2]
	TMSI		NA	NA	25	[3]

[1] *Nat. Commun.* 16, 4586 (2025)*;* [2] *Energy Environ. Sci.* 18, 4800-4810 (2025)*;* [3] *Adv. Energy Mater.* 14, 2402306 (2024).

In our system, the **strong electrostatic field of HVOC drives the formation of a stable organic–inorganic hybrid solid-electrolyte interphase (SEI)** consisting of cation–ZnF_x/ZnS_x complexes at the Zn anode. This interphase effectively regulates Zn deposition kinetics, suppresses parasitic reactions, and stabilizes the Zn interface during extended cycling.

Importantly, we further performed **systematic comparisons among mono-, di-, and tetra-valent cations**. Our results show that monovalent cations can, under certain conditions, achieve Zn anode cycling stability comparable to higher-valent cations. However, when evaluated in full Zn–I_2 batteries, the performance improvement provided by monovalent cations is inferior to that achieved with divalent or tetravalent cations. This observation indicates that while mono-valent cations may partially regulate Zn deposition, their electrostatic interactions are insufficient to simultaneously stabilize polyiodide chemistry at the cathode and Zn metal at the anode. By contrast, the higher charge density of divalent and tetravalent cations generates a much stronger electrostatic field, enabling coupled stabilization of both battery electrodes through effective polyiodide confinement and robust Zn interfacial protection. This dual-interface regulation mechanism ultimately leads to the significantly improved

electrochemical performance observed in the HVOC-based Zn–I_2 batteries.

Therefore, the novelty of this work lies in establishing **cation valence as a fundamental design parameter for electrolyte engineering**, enabling simultaneous regulation of cathode redox chemistry and Zn anode interfacial stability. To the best of our knowledge, such a **valence-governed dual-interface electrolyte design strategy** has not been previously reported for Zn–I_2 battery systems. More specifically, this work demonstrates the **first implementation of high-valent organic cation (HVOC) chemistry in electrolyte design for Zn–I_2 batteries**.

Comments:

1. The author list in the revised manuscript does not match that of the initial version, even resulting in the removal of a corresponding author. This is unreasonable for the lack of previous responsibility.

Response: We thank the reviewer for raising this concern. We would like to clarify that the authorship change was communicated to the editorial office in a transparent manner when the first revised manuscript was submitted. In accordance with the journal's policies on authorship changes, we formally informed the editorial office and submitted the *nr author list change form*, signed by all authors. To ensure full transparency in the present revision round, we will also upload the *nr author list change form* as a supplementary file for review.

As explained in our cover letter submitted with our first-round revision, after careful reconsideration of individual contributions and discussion among all co-authors, Prof. Xiong Wen (David) Lou was removed from the author list and is now acknowledged in the Acknowledgements section. Prof. Lou serves as a mentor to Prof. Jijian Xu through a departmental mentorship program that provides guidance and support to junior faculty members. He advised that it would not be appropriate for him to serve as a co-corresponding author on this work. All authors were informed of and agreed to this change.

2. Regarding the purity of the material, the mass spectrometry (MS) results of HVOC provided by the authors are not considered sufficient proof of the purity. The authors did not provide liquid chromatography (LC) data; MS results can only confirm the presence of the target molecule. For material purity, a combination of ^{1}H NMR, ^{13}C NMR, or possibly ^{15}N NMR would be more conclusive.

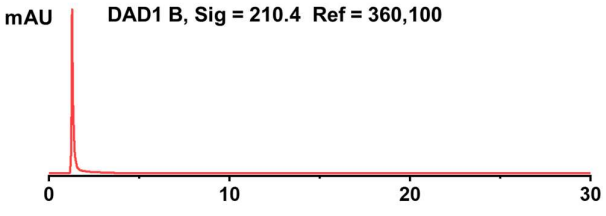

Peak	RetTime	Area (mAU*s)	Height (mAU)	Area (%)
1	1.237	6265.64	924.05	100.00

Fig. R1 Liquid chromatography for $OTA(OTF)_4$.

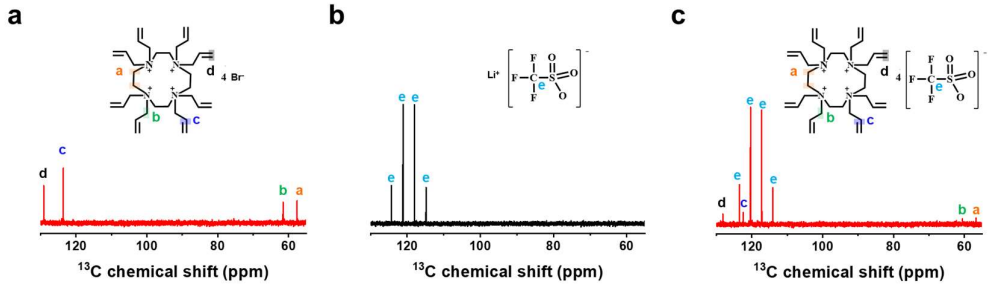

Fig. R2 ^{13}C NMR spectra of **a** $OTABr_4$, **b** LiOTF and **c** $OTA(OTF)_4$.

Response: We thank the reviewer for the valuable suggestion regarding the characterization of the HVOC material purity. In response, we have provided additional characterization data to more comprehensively verify the purity of the synthesized compound. Specifically, liquid chromatography (LC) analysis has been provided in Fig. R1. The LC chromatogram exhibits a dominant peak with no detectable impurity signals, indicating high sample purity. This result, together with the mass spectrometry (MS) data (Supplementary Fig. 4b), confirms the presence of the target species with

high purity. In addition, ^{13}C NMR measurements (Fig. R2) were carried out for $OTABr_4$, LiOTF, and $OTA(OTF)_4$. The carbon signals corresponding to the OTA^{4+} are in good agreement with the structural features reported in the literature (*Energy Environ. Sci. 17, 4519 (2024)*). The ^{13}C NMR spectra of LiOTF and $OTA(OTF)_4$ further support the expected chemical structure and high purity of the product. The slight variation in signal intensity observed in Fig. R2c arises from the use of a zgpg30 pulprog, which is suitable for qualitative analysis but not for quantitative comparison of peak intensities. Moreover, the ^{1}H NMR spectra (Supplementary Fig. 3) are consistent with the reported data, further confirming the molecular structure and high purity of the HVOC material. The corresponding data and discussion have been added to the revised Supplementary Information (Supplementary Figs. 3-4) and to the main text of the revised manuscript (Page 6).

3. In the response file, the authors present R8 c (S64-c), which shows long-term cycling data of Zn–I_2 batteries in different electrolytes. However, the figure indicates that using only $ZnSO_4$ as the salt also enables relatively good cycling performance, remaining stable for 6000 cycles with high and stable Coulombic efficiency. There is no significant difference observed in the initial charge/discharge trends (0-200 cycles) and the subsequent prolonged cycling of base $ZnSO_4$ and HVOC-containing electrolytes. How, then, is the specific role of the additive defined? Conversely, when the authors used $Zn(OTF)_2$ as the salt, the blank electrolyte exhibited worse performance (Fig. 6b). Although the authors mention improved performance at low temperatures, the manuscript is clearly not focused on low-temperature systems.

Response: We thank the reviewer for the careful examination of the cycling data. To clarify this point, we have magnified the cycling data of Fig. S64c (now shown as Fig. R3a) to highlight both the initial cycles (0–200 cycles, Fig. R3b) and the long-term cycling region (5000–6500 cycles, Fig. R3c). As shown in these enlarged views, the Zn–I_2 battery with HVOC consistently exhibits higher capacity retention and more stable Coulombic efficiency (CE) than the blank $ZnSO_4$ electrolyte, both during the

initial cycling stage and throughout prolonged cycling.

Quantitatively, after 6000 cycles, the capacity retention of the cell with the $ZnSO_4$ electrolyte decreases to 75.55%, whereas the HVOC-containing electrolyte maintains 98.82% capacity retention (86.53% relative to the maximum capacity). Moreover, after ~6000 cycles the $ZnSO_4$ electrolyte begins to exhibit noticeable capacity decay and fluctuations in CE, while the HVOC-containing system maintains stable cycling behavior with consistently high CE. These results highlight the long-term stabilizing effect of HVOC on the Zn–I_2 battery system, particularly during extended cycling. To further highlight the role of HVOC in improving the cycling performance, magnified views of the initial cycling region (0–200 cycles) and the long-term cycling region (5000–6500 cycles) have been added to Supplementary Fig. 64. Corresponding discussion has also been incorporated into the revised manuscript (Page 24).

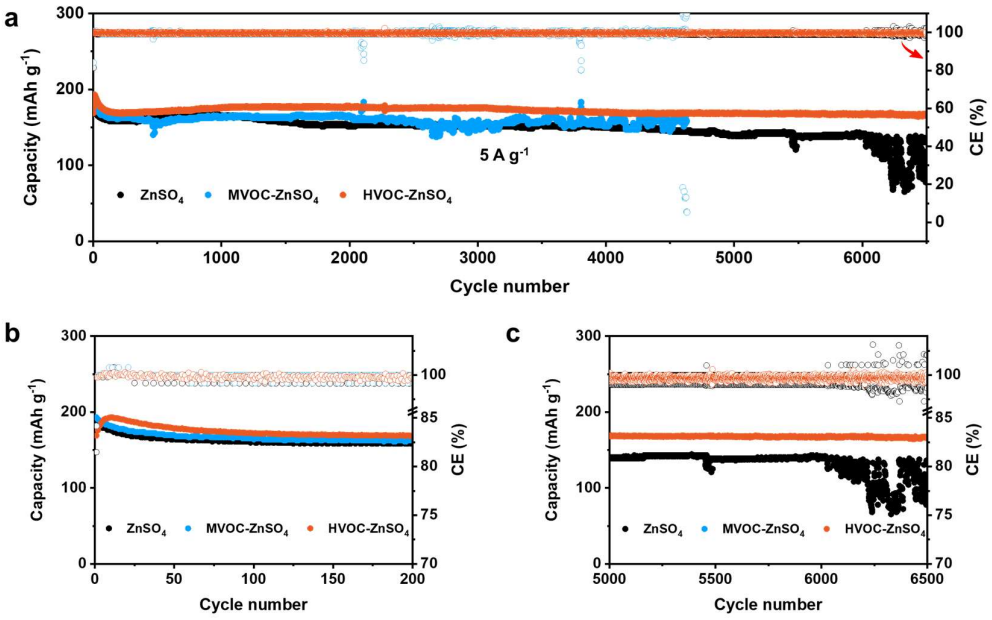

Fig. R3 a Cycling stability of Zn–I_2 battery with HVOC in $ZnSO_4$-based electrolytes. **b** Magnified view of the initial cycling region (0–200 cycles) in **a**. **c** Magnified view of the long-term cycling region (5000–6500 cycles) in **a**.

Regarding the reviewer's question about the $Zn(OTF)_2$ electrolyte, our intention is not to emphasize low-temperature performance alone. In addition, the OTF^- anion is known to facilitate the formation of ZnF_x/ZnS_x-rich interfacial layers on Zn metal, as

widely reported in previous studies (*Nat. Nanotechnol. 16, 902–910 (2021); Angew. Chem. Int. Ed. 62, e202302583 (2023); Matter 7, 4014–4030 (2024); Joule 9, 101844 (2025)*). Such interfacial chemistry is highly relevant to our proposed mechanism, in which the strong electrostatic field of HVOC promotes the formation of an organic–inorganic hybrid solid-electrolyte interphase (SEI) on the Zn anode. Therefore, the $Zn(OTF)_2$-based electrolyte provides a useful platform to further verify the interfacial regulation mechanism proposed in this work. Meanwhile, we agree with the reviewer that the electrochemical performance of Zn–I_2 batteries in different base electrolytes can also be influenced by multiple factors, including anion species, salt concentration, ion conductivity and related properties. These variables represent an important direction for future investigation.

Reviewer #2:

The authors have addressed all my concerns. I appreciate authors' detailed and comprehensive answers, and glad to recommend this work for publication on Nat Commun.

Response: We sincerely appreciate the reviewer's positive assessment of our revised manuscript. We are glad that the revisions and responses have adequately addressed the previous concerns and that the manuscript is now considered suitable for publication.

Reviewer #3:

I have reviewed the response, all my concerns have been addressed properly. I have no more questions.

Response: We sincerely thank the reviewer for the positive feedback and for confirming that the previous concerns have been satisfactorily addressed. We appreciate the reviewer's time and insightful suggestions.